AD-A065 301 CALIFORNIA INST OF TECH PASADENA GRADUATE AERONAUTIC--ETC F/G 20/13
NONLINEAR INTERACTIONS IN SUPERFLUID DYNAMICS: SUPERCRITICAL CO--ETC(U)
NOV 78 H W LIEPMANN, P L ROGERS, T N TURNER F44620-75-C-003A
UNCLASSIFIED AFOSR-TR-79-0130 NL

1 OF 2
AD
A065301

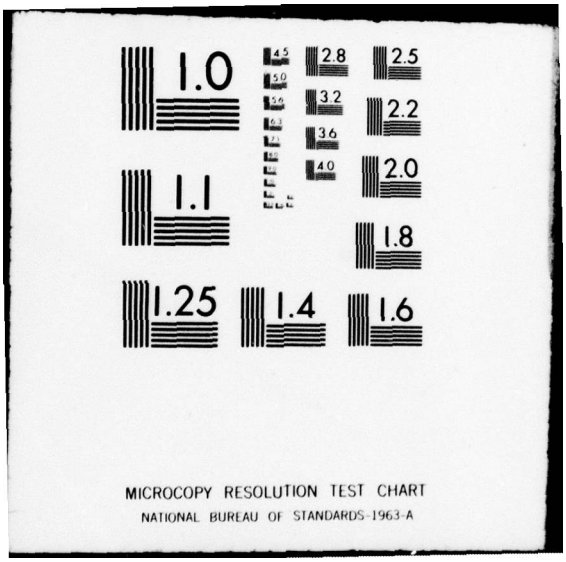
1.0
1.1
1.25
1.4
1.6
1.8
2.0
2.2
2.5
2.8
3.2
3.6
4.0
4.5
5.0
MICROCOPY RESOLUTION TEST CHART
NATIONAL BUREAU OF STANDARDS-1963-A

(18) AFOSR-TR--79-0130

(14) LEVEL II

(9) FINAL SCIENTIFIC REPORT,

AFOSR Contract F44620-75-C-0038

(15)

(6) NONLINEAR INTERACTIONS IN SUPERFLUID DYNAMICS: SUPERCRITICAL COUNTERFLOW AND SHOCKWAVES,

by

(10) H. W./Liepmann, Philip L./Rogers,
Timothy N./Turner, Jack L./Wise

Submitted by:

H. W. Liepmann
Director of GALCIT

(16) 2301

(17) A5

(12) 114p.

GRADUATE AERONAUTICAL LABORATORIES
CALIFORNIA INSTITUTE OF TECHNOLOGY
PASADENA, CALIFORNIA

(11) 30 November 30, 1978

157 700 LB

TABLE OF CONTENTS

SECTION A

NONLINEAR INTERACTIONS IN SUPERFLUID DYNAMICS: SUPERCRITICAL COUNTERFLOW AND SHOCKWAVES

I. INTRODUCTION

With the present final report the AFOSR support for the GALCIT research on liquid helium fluid dynamics terminates. The three sections included here describe the work done during the last contractual period up to September 30, 1978.

It was the purpose of the program to investigate some aspects of the fluid mechanics of LHeII, in particular nonlinear phenomena such as turbulence and shock waves and their effect on the critical conditions in HeII.

The major accomplishments which resulted from this GALCIT research program are listed below. The larger part of the work was supported by contracts from AFOSR which are gratefully acknowledged. A list of publications is included with the report.

II. PRINCIPAL ACCOMPLISHMENTS

1. The development of the first cryogenic shock tube for the production of strong shock waves. In this small (1" diameter) tube, shock Mach numbers of $M = 42$ in Helium gas have been reached. The cooling effect on density and viscosity is such that the Reynolds number of the tube is very high and boundary layer displacement effects in the shock wave propagation negligible. Indeed, to obtain similar Reynolds number at room temperature a tube about 1000 times the present tube diameter would be required. (Of course, a tube at room temperature would be restricted to relatively low Mach numbers because of real gas effects, e.g., ionization.) The potential use of this cryogenic shock tube has not nearly been exhausted. To mention only one, a recent possibly important application would be the study of wall ablation in the wake of very strong shocks, suggested by problems arising from the MX development.

2. The extension of the cryogenic tube techniques to work with liquid Helium II led to the first careful mapping of the nonlinear wave diagrams in He II, involving both first sound and second sound shock waves. These measurements permit the first rational comparison of theory and experiment for nonlinear flow phenomena in LHe.

3. Ultra-second sound waves with frequencies up to 1 MHz have been used as a velocimeter for He II counterflow. The first recorded observations of turbulent-like velocity fluctuations was carried out here using this technique. This work was made possible by the development of superconducting temperature sensors with 10^{-8} ^{o}K sensitivity. Possible application to IR detection is clear. Indeed, this second sound technique permitted the first direct measurements of a flow velocity in He II.

4. A similarity rule was developed based on the two-fluid equation with the additional Gorter-Mellink terms. This rule permits the reduction of all known critical heat flow experiments in capillaries and tubes to a single number reminiscent of a critical Reynolds number for laminar-turbulent transition in classical fluid mechanics.

5. Critical counterflow velocities and hence critical heat flow two orders of magnitude larger than previously reported for similar geometries have been measured in the wake of second sound shock waves.

GALCIT Publications on Liquid Helium and Cryogenic Fluid Mechanics

1. J. E. Broadwell and H. W. Liepmann, Local Boiling and Cavitation in Heat-Induced Counterflow of He II, Physics of Fluids 2, 8, August 1969.

2. P. E. Dimotakis, Investigation of Supercritical Heat Flow in Helium II, Ph. D. Thesis, California Institute of Technology October 1972.

3. V. C. Rupert, Experimental Study of Shock Wave Strengthening by a Positive Density Gradient in a Cryogenic Shock Tube, Ph. D. Thesis, California Institute of Technology, May 1972.

4. H. W. Liepmann, J. C. Cummings, and V. C. Rupert, Cryogenic Shock Tube, Physics of Fluids 16, 2, February 1973.

5. P. E. Dimotakis and J. E. Broadwell, Local Temperature Measurements in Supercritical Counterflow in Liquid Helium II, Physics of Fluids 16, p. 1787, November 1973.

6. J. C. Cummings, I. Development of a Cryogenic Shock Tube, II, Experimental Investigation of the Interaction of a Shock Wave with Liquid Helium I & II. Ph. D. Thesis, California Institute of Technology, May 1973.

7. H. W. Liepmann, Cryogenic Fluid Mechanics, Recent Developments in Shock Tube Research, Daniel Bershader and Wayland Griffith, Editors, Stanford University Press, July 1973.

8. J. C. Cummings, Development of a High-Performance Cryogenic Shock Tube, J. Fluid Mech. v. 66, part 1, pp. 177-187 (1974).

9. V. C. Rupert, Experimental Study of Shock Wave Strengthening by a Positive Density Gradient in a Cryogenic Shock Tube, Physics of Fluids 17, 9, September 1974.

10. P. E. Dimotakis, Gorter-Mellink Scale, and Critical Velocities in Liquid-Helium-II Counterflow, Physical Review A, v. 10, No. 5, November 1974.

11. G. Laguna and P. E. Dimotakis, Second Sound Attenuation in a Counterflow Jet, APS Bulletin 19, 1161 (1974).

12. G. Laguna and A. Lidow, Shock Waves in Liquid Helium, APS Bulletin 19, 1962 (1974).

13. G. A. Laguna, Second Sound Attenuation in a Liquid Helium Counterflow Jet, Ph. D. Thesis, California Institute of Technology, March 1975.

14. H. W. Liepmann, Fluid Dynamics of Liquid Helium, SIAM J. Appl. Math. 28, No. 3, May 1975.

15. G. Laguna, Second Sound Attenuation in a Supercritical Counterflow Jet, Physical Review B, 12, 11, December 1975.

16. G. Laguna, Photolithographic Fabrication of High Frequency Second Sound Detectors, Cryogenics, April 1976 pp. 241-3.

17. J. B. Smith and G. A. Laguna, Second Sound Spectroscopy: A New Method for Studying Optical Absorption in Solids, Physics Letters, v. 56A, No. 3, March 1976, p. 223-4.

18. J. C. Cummings, Experimental Investigation of Shock Waves in Liquid Helium I & II, Journal Fluid Mech., v. 75, part 2, pp. 373-383 (1976).

19. P. E. Dimotakis and Glenn A. Laguna, Investigations of Turbulence in a Liquid Helium II Counterflow Jet, Physical Review B, 15, 11, June 1977.

20. J. L. Wise, Experimental Investigation of First- and Second-Sound Shock Waves in Liquid Helium II, APS Bulletin 23, No. 8, p. 1015, October 1978.

21. T. N. Turner, Theoretical Calculation of Second Sound Shock Wave Structure in Liquid Helium II, APS Bulletin 23, No. 8, p. 1015, October 1978.

SECTION B

Experimental Investigation of First- and Second-Sound Shock Waves in Liquid Helium II

SECTION B

EXPERIMENTAL INVESTIGATION OF FIRST- AND SECOND-SOUND SHOCK WAVES IN LIQUID HELIUM II

I. INTRODUCTION

An important aspect of the liquid helium research performed at GALCIT began with the initial investigations by Cummings (1973, 1976) of the production and propagation of finite-amplitude disturbances--shock waves--in Liquid Helium II (LHeII). Current efforts include attempts to both refine and expand upon these initial measurements.

Using the two-fluid equations (Landau 1941) for the hydrodynamics of helium II, Khalatnikov (1952, 1965) has derived expressions governing the propagation of weak shock waves by considering terms up to second order in the relative velocity $\bar{w}$ between the normal fluid and superfluid ($\bar{w} = \bar{v}_n - \bar{v}_s$). The present experiments involve the development of techniques which make it possible to assess the accuracy of Khalatnikov's predictions and to estimate the magnitude of the temperature discontinuities associated with shock waves in LHeII.

II. EXPERIMENTAL APPARATUS AND PROCEDURE

Cryogenic Shock Tube

The 1-inch diameter cryogenic shock tube (Liepmann, Cummings, & Rupert 1973; Cummings 1973, 1974), shown in Figure 1, is used to generate a gasdynamic shock which propagates through saturated helium vapor and subsequently reflects from the upper surface of a column of LHeII at the lower end of the test section. A gasdynamic shock produces jumps in temperature and pressure which

are functions only of the shock Mach number. These well-defined jumps provide initial conditions for the production of shocks in the liquid. Beginning with a measurement of the Mach number of the incident gasdynamic shock, one can use the shock jump relations for an ideal gas and the Khalatnikov model for weak shocks in LHeII, together with matching conditions for pressure and velocity at the vapor-liquid interface, to predict wave trajectories in the liquid. These theoretical trajectories may then be compared to experimentally observed values.

x-t Diagrams

The reflection of a gasdynamic shock from the vapor-liquid interface results in a complicated set of finite-amplitude waves whose trajectories are best illustrated by the wave diagram shown in Figure 2. In this diagram, the arrival time of the waves, t, is plotted as a function of position, x. The arrival of the incident gas shock at the liquid surface results in a reflected gasdynamic shock with velocity U_R, and produces two transmitted shocks which propagate into the liquid. One of these shocks is a pressure, or first-sound, shock with velocity $C_1(0)$; the other shock is a temperature, or second-sound, shock with velocity $C_2(6)$. Compression of the liquid by the pressure shock results in a bulk fluid velocity, u_6, which is evidenced by the motion of the vapor-liquid interface. The pressure shock is reflected from the solid endwall and returns to the liquid surface where it is re-reflected as an expansion in the liquid and produces a transmitted gasdynamic shock in the vapor. The reflected and re-reflected pressure waves in the liquid interact with the temperature shock and produce changes in the bulk fluid velocity.

Detector Array

The current experiments involve the accurate measurement of the arrival times of the various waves at detectors located at different heights above and below the liquid surface. Two types of detector are used. Side-mounted, carbon-card detectors, similar to those used in the original work of Cummings, are used to measure the arrival of the incident and reflected gasdynamic shocks. To measure the arrival of either the incident gas shock in the vapor, or the arrivals of the various waves in the liquid, superconducting thin-film gages have been developed to replace the carbon-flake detectors used by Cummings. The new gages are produced by evaporation of aluminum in an oxygen atmosphere and are located on the tips of pyrex rods which project upward from the shock tube endwall. The overall array of detectors represents a blockage of 13% of the cross-sectional area of the shock tube.

The superconducting gages afford major improvements in frequency response and sensitivity over previous detectors. Sensitivities as high as 0.1 to 1.0 $V/^{o}K$ and frequency response on the order of 1.0 MHz have been achieved. The high sensitivity of the present gages is evidenced in Figure 3 which shows the voltage drop across a film as a function of temperature. Each curve in Figure 3 represents the superconducting transition for a different value of externally-applied magnetic field. By increasing the magnetic field, the transitions are biased to lower temperatures. For a given set of shock tube runs, the external magnetic field is adjusted such that the mid-transition point of the films corresponds to the desired initial temperature and pressure. For the film calibration shown in Figure 3, the mid-

transition sensitivity is seen to vary from 0.13 V/°K for the highest transition temperature to 0.039 V/°K for the lowest transition temperature.

Liquid Level Detection

The high sensitivity of these films provides the previously unrealized ability to accurately determine the liquid level in the shock tube prior to actually firing the shock. This new level detection scheme involves the generation of a second-sound pulse at the endwall and the subsequent measurement of the time of flight of the pulse from a submerged superconducting film to the free surface and back to the film. Knowledge of the second-sound wave speed and the height of the detector above the endwall then permits straightforward calculation of the liquid level. Figure 4 shows a typical pair of oscilloscope traces obtained during a level-detection run. In this case, the free surface of the liquid is 44 mm above the endwall; film#3 is 38 mm above the endwall; and film#4 is 34 mm above the endwall. The passages of the upward-travelling pulse and the returning reflection are clearly evident in each trace.

Detector Response

Typical outputs from the present set of shock tube detectors following the actual firing of a gasdynamic shock are shown in Figures 5 and 6. The upper two traces in Figure 5 show the response of two superconducting gages which were initially above the liquid surface to the passage of the incident gasdynamic shock. The bottom trace in Figure 5 shows the response of the carbon-card detector to the passage of the incident and reflected gasdynamic shocks. The traces shown in Figure 6 correspond to the outputs of two superconducting films initially located below

the liquid surface. The film#3 output indicates the sequential arrival of the incident pressure shock, temperature shock, reflected pressure shock, and re-reflected expansion. Film#4, which was initially located somewhat further below the liquid surface than film#3, indicates the sequential arrival of the incident pressure shock, reflected pressure shock, re-reflected expansion, and temperature shock. The detector signals qualitatively verify theoretical predictions that, within the superfluid, the temperature decreases through the pressure shock and increases through the temperature shock.

III. EXPERIMENTAL RESULTS AND OBSERVATIONS

$\chi - \tau$ Diagrams

Sets of photographs similar to those shown in Figures 5 and 6 are taken for a variety of liquid depths at a given saturation pressure and temperature. Arrival time data obtained from these photographs then permits the construction of x-t diagrams by use of the similarity parameters χ and τ given by:

$$\chi = \frac{L - x}{L}$$

$$\tau = \frac{t - T}{L} \quad (\mu\text{sec/cm})$$

where x = height above endwall (cm)
t = arrival time (μsec)
L = initial liquid depth (cm)
T = arrival time of incident gasdynamic shock at liquid surface (μsec)

At the present time accurate $\chi - \tau$ diagrams have been constructed for seven initial liquid temperatures and pressures. These diagrams are shown in Figures 7-13 for the cases $\overline{T}_1$ = 1.522, 1.665, 1.751, 1.832, 1.989, 2.031, and 2.095^{o}K, respectively.

The Mach number of the incident gas shock ranged from $\overline{M}_S = 13.0$ for the case $\overline{T}_1 = 1.522^{\circ}K$, to $\overline{M}_S = 6.52$ for the case $\overline{T}_1 = 2.095^{\circ}K$. All of the diagrams clearly indicate arrival time data for the various waves discussed earlier. Excellent repeatability of the arrival time measurements is evident in each $\chi - \tau$ diagram. Linear fits to the data indicate standard deviations in experimentally measured velocities on the order of one to two percent.

Wave Velocities

Figure 14 is a comparison of experimental wave velocities obtained from the $\chi - \tau$ measurements to theoretical velocities computed on the basis of the strength of the incident gas shock. As mentioned earlier, the theoretical computations treat the vapor as an ideal gas and assume that the propagation of a first-sound shock is adequately modeled by Khalatnikov's second-order theory. The theoretical velocity of a second-sound shock in a particular region is taken to be equal to the sum of the bulk fluid velocity of that region and the second-sound velocity corrected for the region pressure.

In Figure 14, the ratios of experimentally observed velocities to theoretical velocities are shown. Good agreement between theory and experiment is obtained for the incident pressure shock velocity, $C_1(0)$. Measurements of the reflected pressure shock velocity, $C_1(6)$, and the temperature shock velocity, $C_2(6)$, are low and exhibit decreasing agreement with theory as the initial temperature and pressure are increased. The bulk fluid velocity, $u_5 = u_6$, is obtained from the experimental data by taking the inverse slope of the line connecting the origin of the $\chi-\tau$ diagram to a point corresponding to the intersection of the reflected pressure shock data with the re-reflected ex-

pansion data. The resultant values obtained for $u_5 = u_6$ deviate significantly from theory--they are 30-58% low for the cases examined.

Phase Diagram

The initial conditions for each set of χ-τ measurements and the subsequent states of the liquid following the passage of the pressure waves are best illustrated by the phase diagram shown in Figure 15. Each run starts with the liquid-vapor system in equilibrium along the saturated vapor curve. The incident pressure shock raises the pressure of the liquid to p_6, the reflected pressure shock increases the pressure still further to p_7, and the re-reflected expansion reduces the pressure to p_8. To first order it is assumed that there is no temperature change across these waves.

Phase Transitions

From the phase diagram, it is apparent that for initial conditions sufficiently close to the lambda transition the pressure jump across either the incident pressure shock or reflected pressure shock is sufficient to cause a change in phase of the liquid from LHeII to LHeI. This predicted change in phase has been experimentally evidenced by detector outputs indicating the disappearance of temperature shocks in the wakes of sufficiently strong pressure shocks. For the case of $\overline{T}_1 = 2.095^{\circ}K$, shown in Figure 13, the χ-τ measurements indicate the disappearance of the temperature shock following the passage of the incident pressure shock through the liquid. This result is significant and indicates that the transition from LHeII to LHeI occurs within the propagating pressure shock.

Observation of the phase diagram also indicates the possi-

bility of firing gasdynamic shocks of sufficient strength to drive the state of the fluid across the melting line into the solid region from either the LHeII or LHeI region. Experiments of this nature would involve straightforward modification of the present apparatus to achieve significantly higher driver pressures, p_4, than the present range of p_4 = 4-5 Atm. For p_6 to exceed the melting pressure, initial estimates indicate required values of p_4 greater than 30 Atm for $T_o = T_1 = 2.10^oK$, or greater than 45 Atm for $T_o = 1.65^oK$. If the reflected pressure shock is instead relied upon to produce values of p_7 that surpass the melting pressure, the minimum requirement for p_4 drops to roughly 10 Atm. Optical techniques may be employed for investigations of condensation phenomena associated with strong pressure shocks.

Temperature Jumps & Relative Velocity Estimates

Referring to Landau and Lifshitz (1959, p. 519), the relative velocity produced by passage of a first-sound wave may be expressed to first order in the temperature jump as

$$w = v_n - v_s = \frac{\rho s}{\rho_n C_{10}} \Delta T$$

where s = entropy
ρ = density
ρ_n = normal fluid density
C_{10} = first-sound wave speed
ΔT = temperature jump

In the present set of measurements, values of $\Delta T \approx -30 \times 10^{-3}\ ^oK$, which correspond to $w \approx -0.15$ m/sec, were obtained for the incident pressure shock.

In the case of second-sound shocks, Khalatnikov (1965, p. 83) has written

$$w = \frac{\rho s}{\rho_n C_{20}} \Delta T$$

where C_{20} = second-sound wave speed

Using side-mounted aluminum oxide films for the case $\bar{T}_o = 1.788^{\circ}K$, shock tube measurements indicate $\Delta\bar{T} = 25 \times 10^{-3}\ ^{\circ}K$ for the second-sound shock produced by reflection of a gasdynamic shock from the free surface of the liquid. This temperature jump corresponds to w = 2.2 m/sec--a value which agrees well with critical velocity measurements of w_c = 2.51 m/sec obtained using temperature shocks produced by delivering electrical pulses to a thin-film heating element (Rogers 1978). These values of w_c are two orders of magnitude larger than those reported for steady channel flow (e.g., see Dimotakis 1974).

IV. CONCLUSIONS

The experimental work reported here demonstrates the development of instrumentation and techniques suitable for making accurate and repeatable measurements of shock arrival times and estimates of shock-induced temperature jumps in LHeII. Arrival time measurements indicate consistent discrepancies between theoretical predictions and experimental results for u_6 and the wave trajectories. The discrepancies may be related to shortcomings of Khalatnikov's second-order theory or to mass-transfer effects at the vapor-liquid interface. These possibilities are being further examined. Measurements of temperature jumps associated with first-sound shocks show approximate agreement with theoretical predictions. Experimental measurements of temperature jumps associated with the coupled second-sound shock indicate limitation of the magnitude of the temperature discon-

tinuity by the development of a critical relative velocity on the order of 2.2 m/sec.

The present experimental data indicate that a phase transition from LHeII to LHeI can be produced by sufficiently strong first-sound shocks for initial test conditions close to the lambda transition. Using stronger shocks, it should be possible to drive the state of the liquid across the melting line into the solid region from either the LHeII or LHeI region. Due to the relatively low pressures associated with the solid phase, liquid helium is a promising candidate for potential studies of shock-induced liquid-solid condensation.

V. REFERENCES

1. Cummings, J.C., "Part I, Development of a Cryogenic Shock Tube; Part II, Experimental Investigation of the Interaction of a Shock Wave with Liquid Helium I and II," Ph.D. Thesis, California Institute of Technology, Pasadena, 1973.

2. Cummings, J.C., "Development of a High-Performance Cryogenic Shock Tube," J. Fluid Mech., Vol. 66, Part 1, pp. 177-187, 1974.

3. Cummings, J.C., "Experimental Investigation of Shock Waves in Liquid Helium I and II," J. Fluid Mech., Vol. 75, Part 2, pp. 373-383, 1976.

4. Dimotakis, P.E., "Gorter-Mellink Scale, and Critical Velocities in Liquid-Helium-II Counterflow," Phys. Rev. A, Vol. 10, No. 5, pp. 1721-1723, Nov. 1974.

5. Khalatnikov, I.M., "Discontinuities and High Amplitude Sound in Helium II," Zh. Eksperim. i Teor. Fiz., Vol. 23, pp. 253-264, 1952.

6. Khalatnikov, I.M., Introduction to the Theory of Superfluidity, New York: W.A. Benjamin, Inc., 1965.

7. Landau, L.D., "The Theory of Superfluidity of Helium II," J. Phys. USSR, Vol. V, No. 1, pp. 71-90, 1941.

8. Landau, L.D., and E.M. Lifshitz, Fluid Mechanics, London: Pergamon Press, 1959.

9. Liepmann, H.W., J.C. Cummings, and V.C. Rupert, "Cryogenic Shock Tube," Phys. Fluids, Vol. 16, No. 2, pp. 332-333, Feb. 1973.

10. Rogers, P.L., "Experimental Investigation of Second Sound Shock Waves in Liquid Helium II," Ae.E. Thesis, California Institute of Technology, Pasadena, 1978.

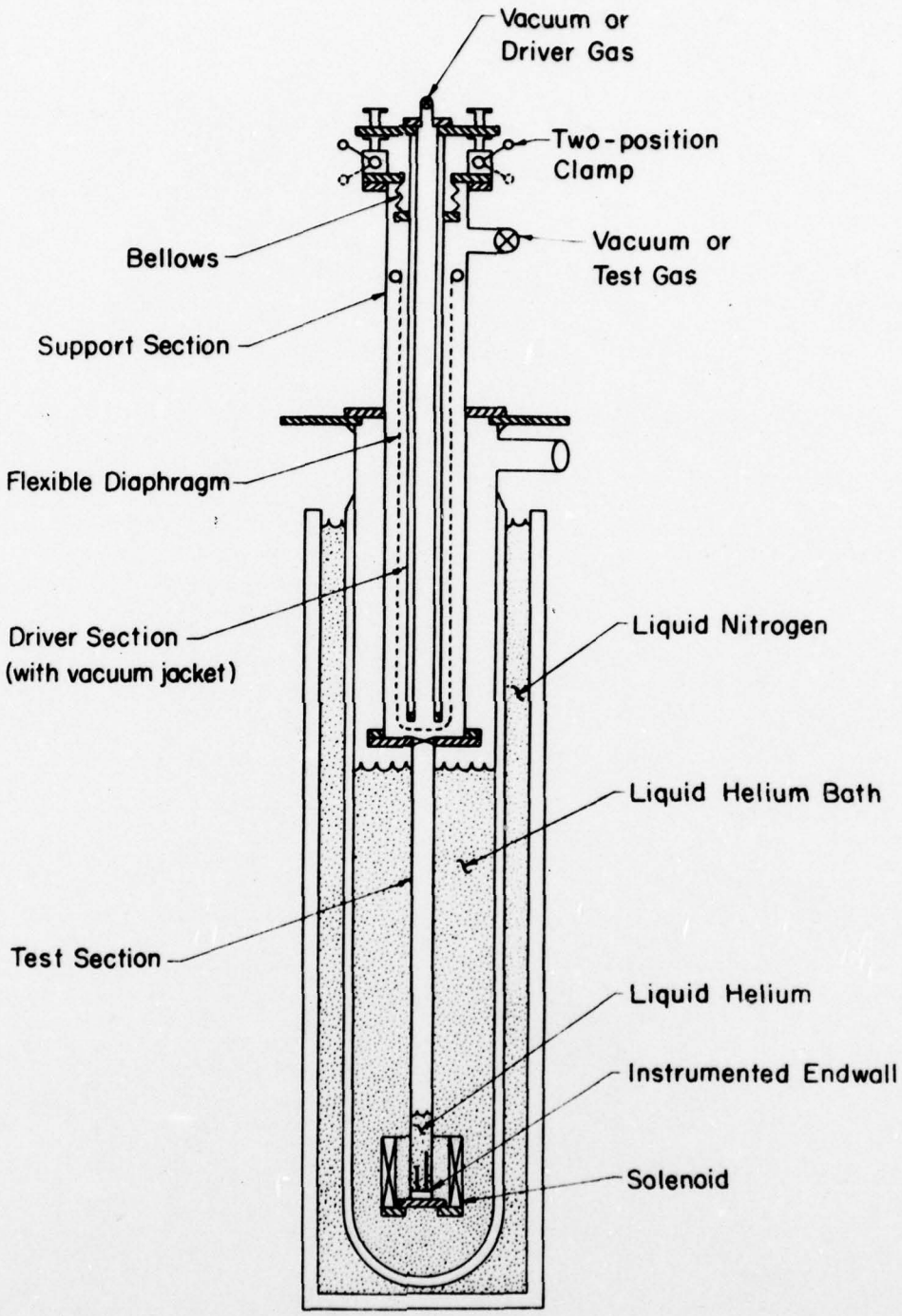

CRYOGENIC SHOCK TUBE ASSEMBLY

Figure 1

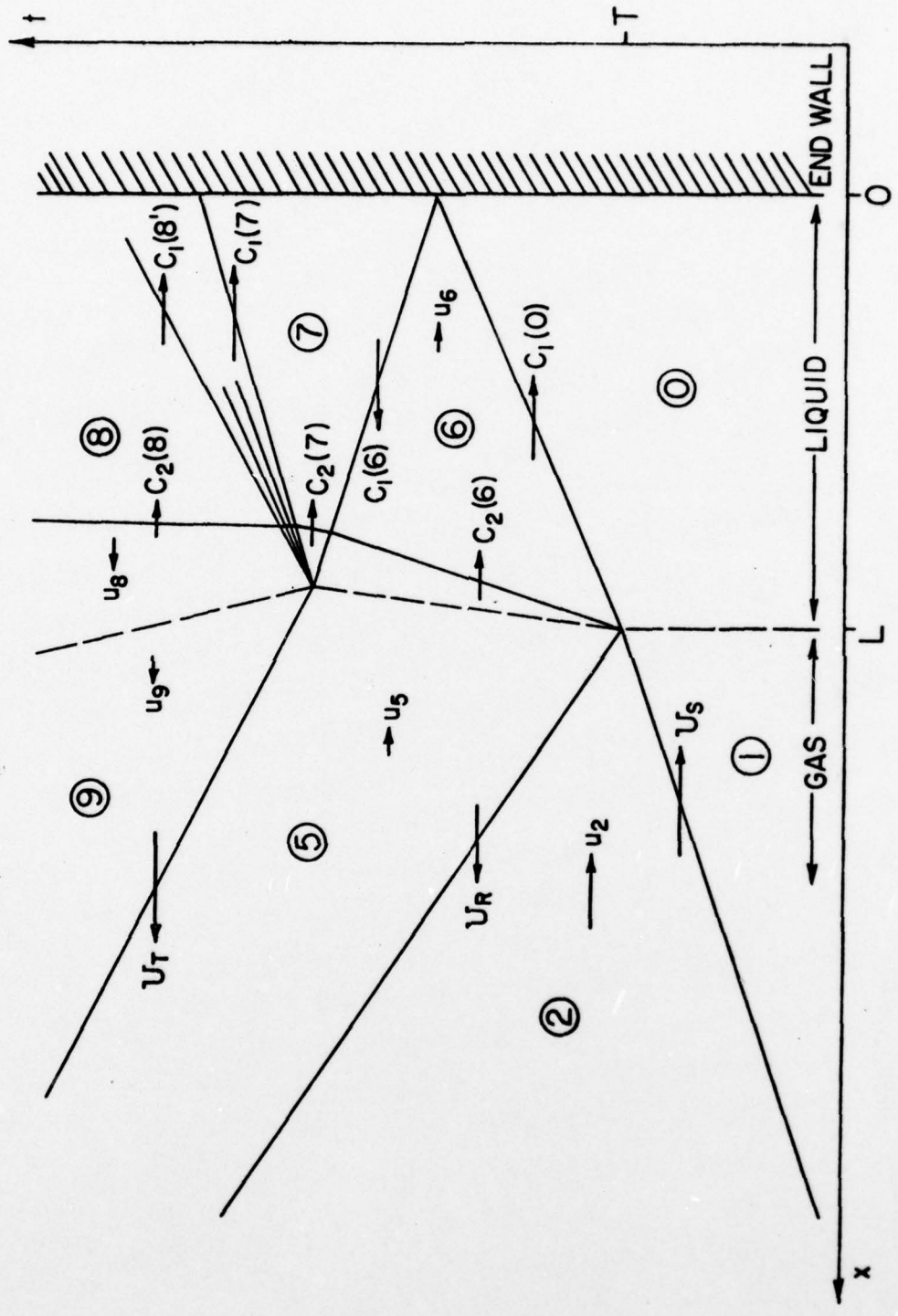

Figure 2: x-t Diagram Notation

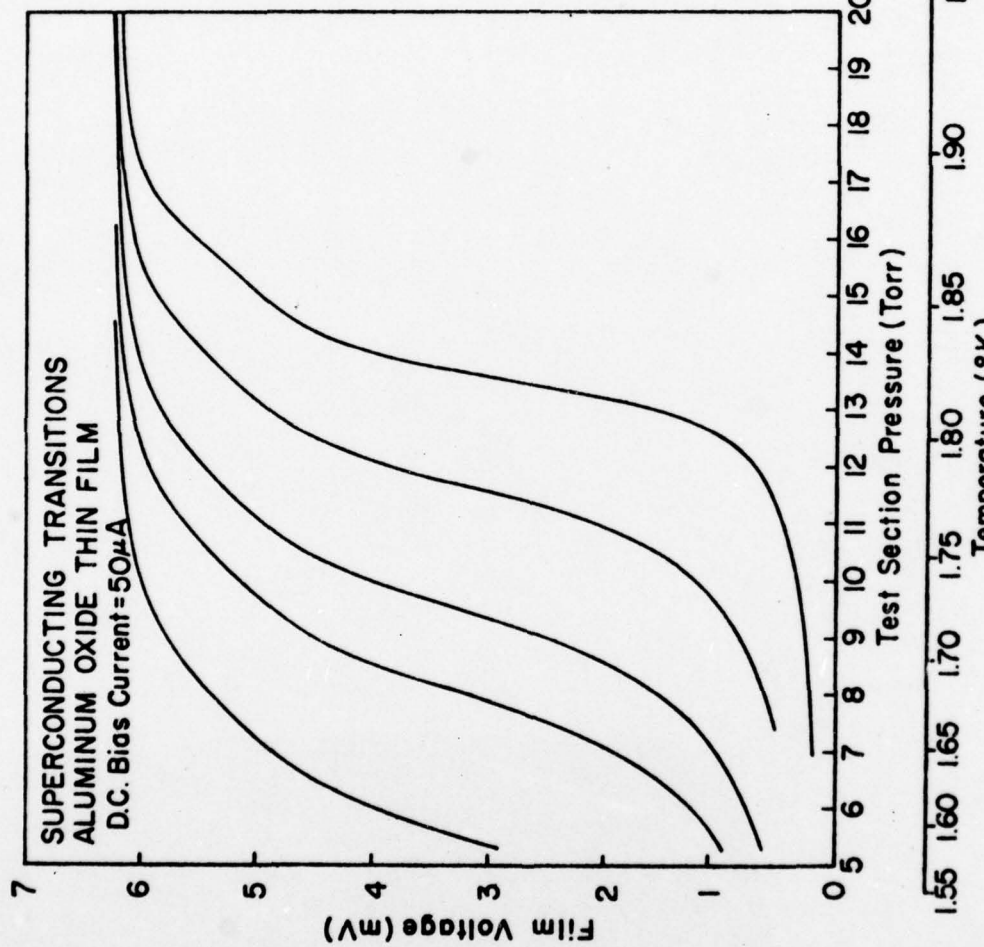

Figure 3: Superconducting Detector Calibration

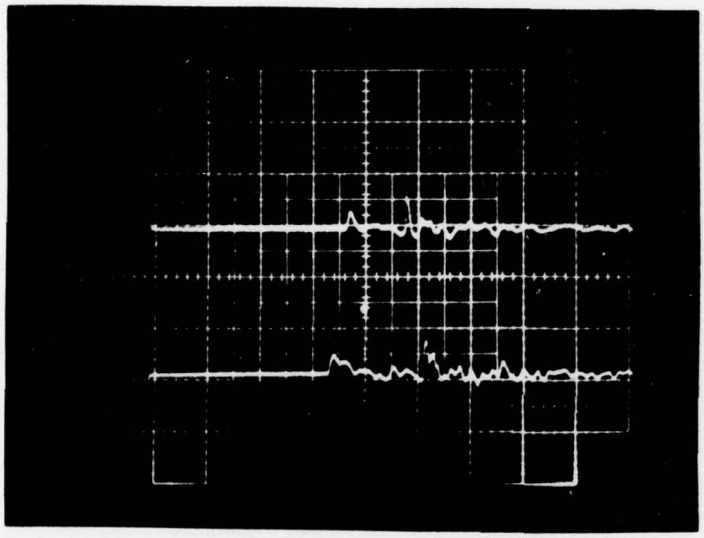

FILM 3
.4mV/div
.5msec/div

FILM 4
.4mV/div
.5msec/div

1/14/78, RUN 55
$P_1 = P_{s.v.} = 7.51$ torr
$T_1 = 1.666°K$

Figure 4: Typical Level-Detection Run

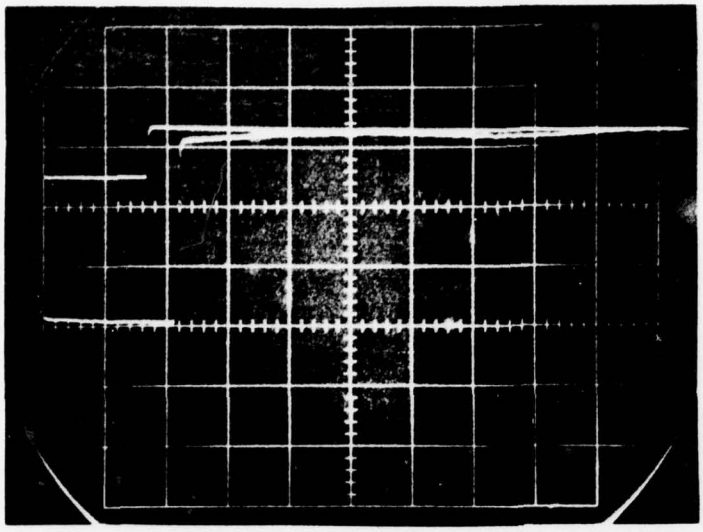

FILM 1
5 mV/div
10 μ sec/div

FILM 2
2mV/div
10 μ sec/div

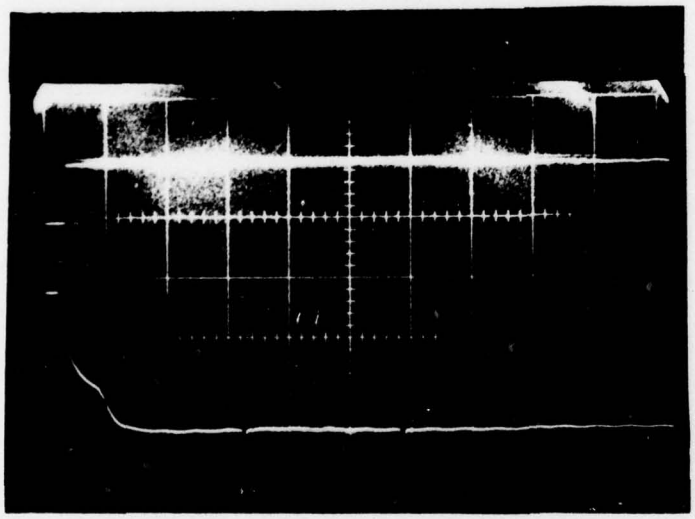

FILM 1
5mV/div
50 μ sec/div

CARBON CARD
DETECTOR
.1V/div
50 μ sec/div

1/14/78, RUN 56
$P_1 = P_{s.v.} = 7.40$ torr
$T_1 = 1.663\,^{\circ}K$

Figure 5: Detector Response to the Vapor Flow Field

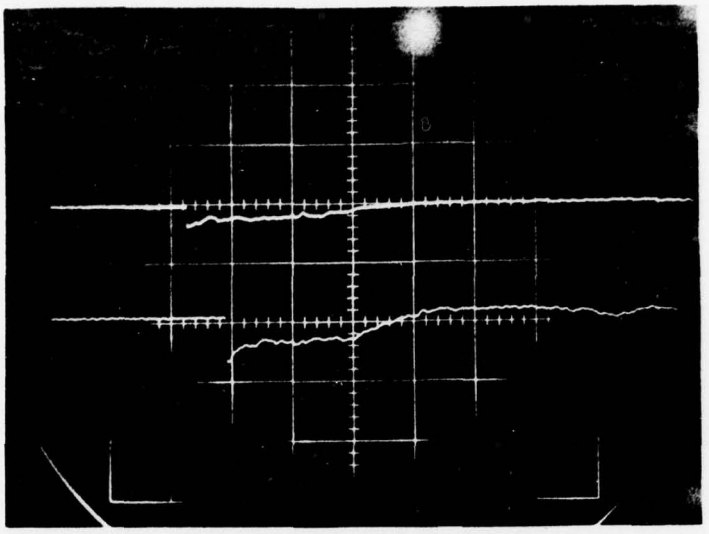

FILM 3
2mV/div
20 μ sec/div

FILM 4
2mV/div
20 μ sec/div

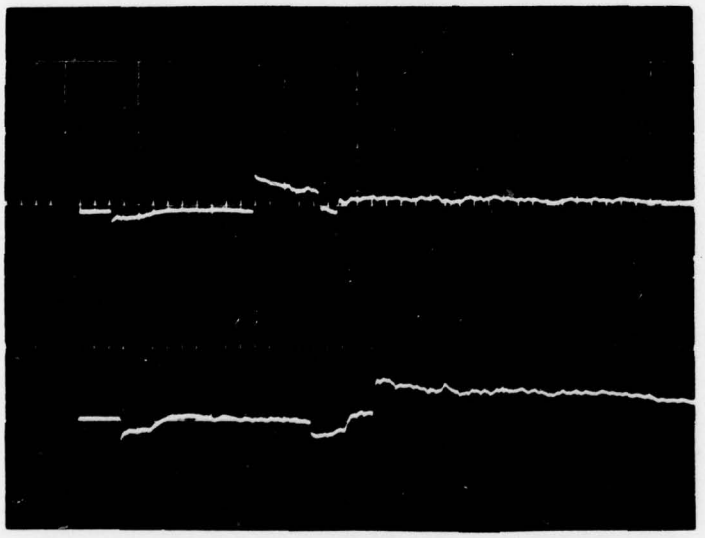

FILM 3
5mV/div
100 μ sec/div

FILM 4
5mV/div
100 μ sec/div

1/14/78, RUN 56
$P_1 = P_{s.v.} = 7.40$ torr
$T_1 = 1.663\,^{\circ}K$

Figure 6: Detector Response to the Liquid Flow Field

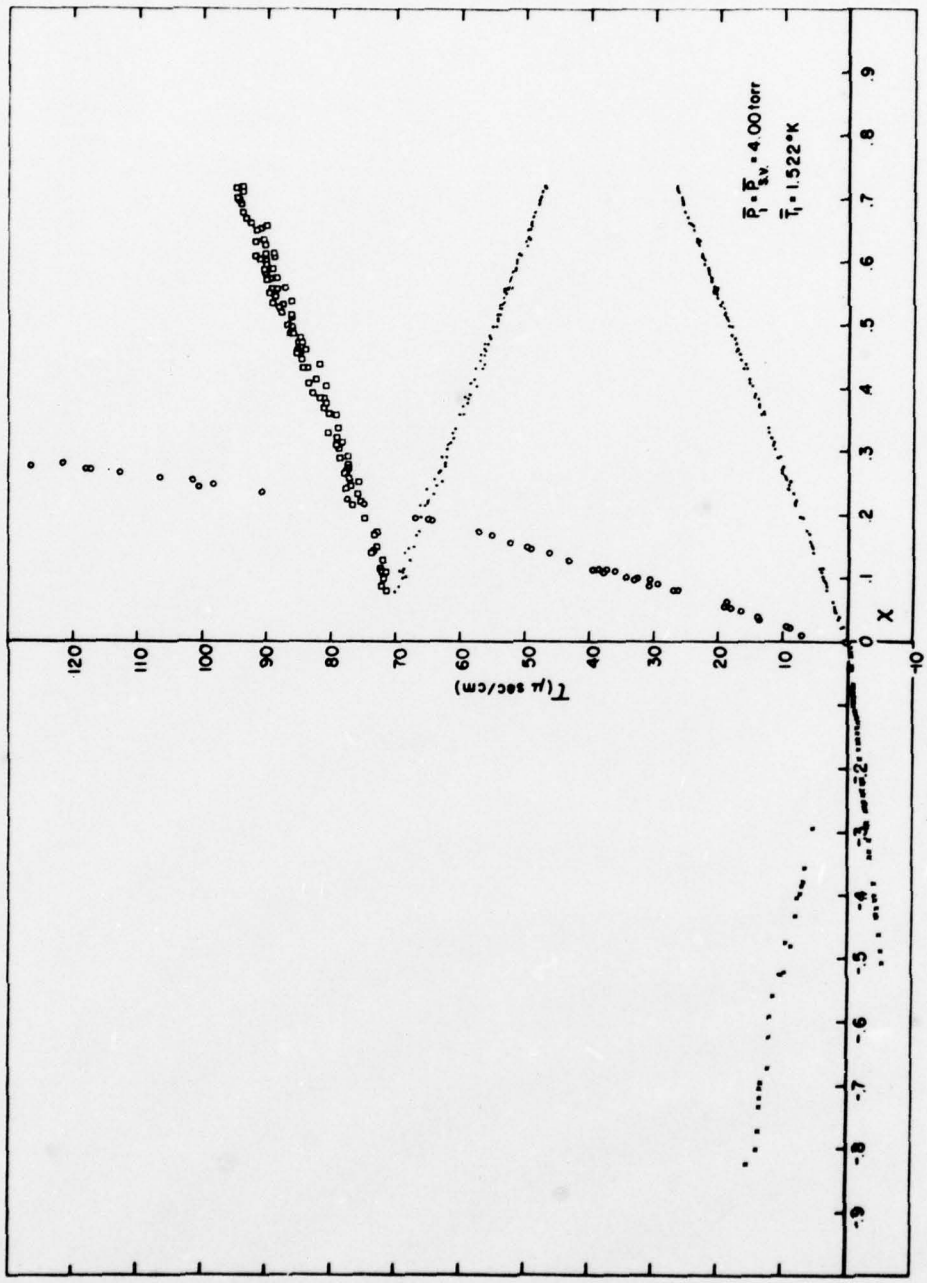

Figure 7: $\chi - \tau$ Diagram for $\bar{T}_1 = 1.522^{o}K$

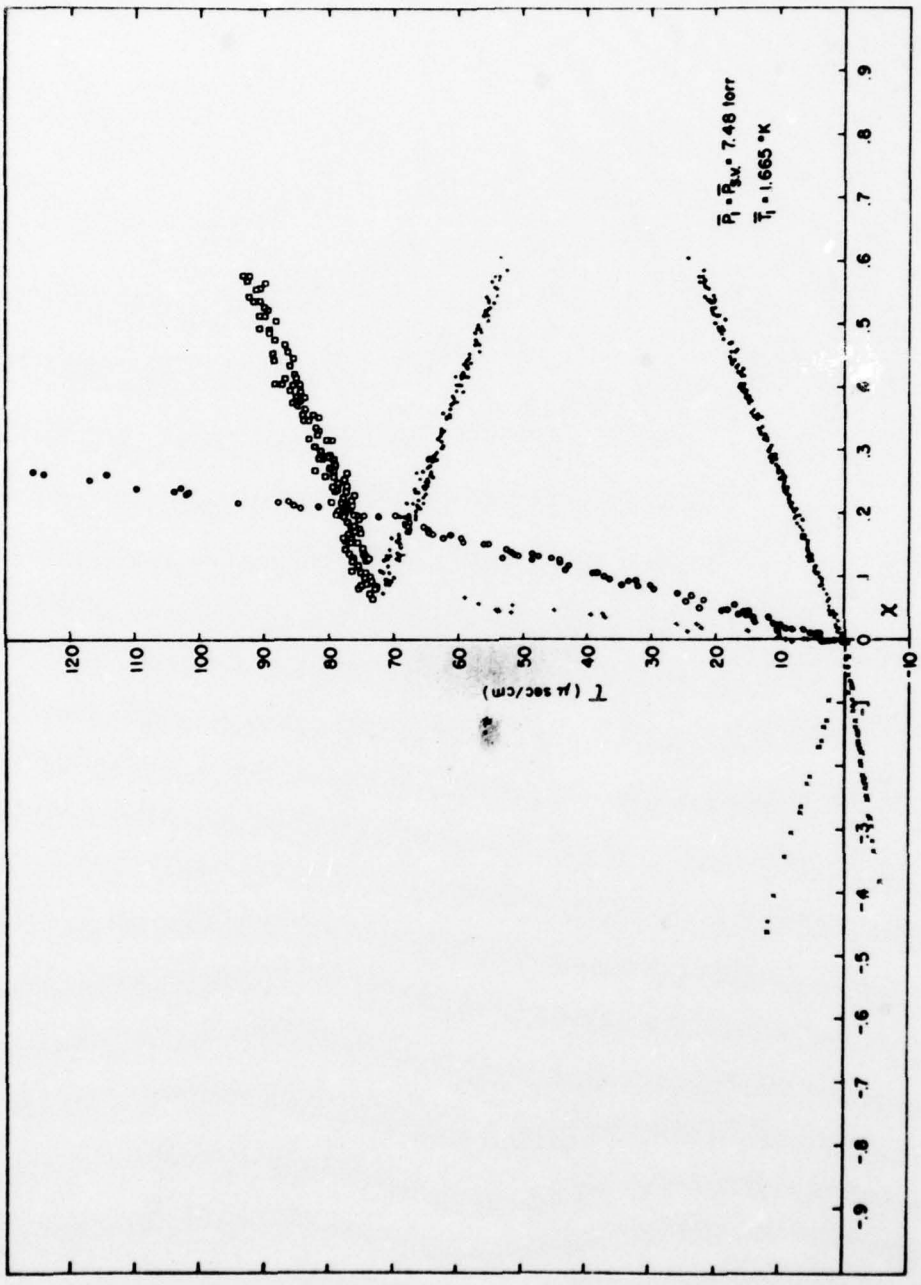

Figure 8: X − τ Diagram for $\bar{T}_1$ = 1.665°K

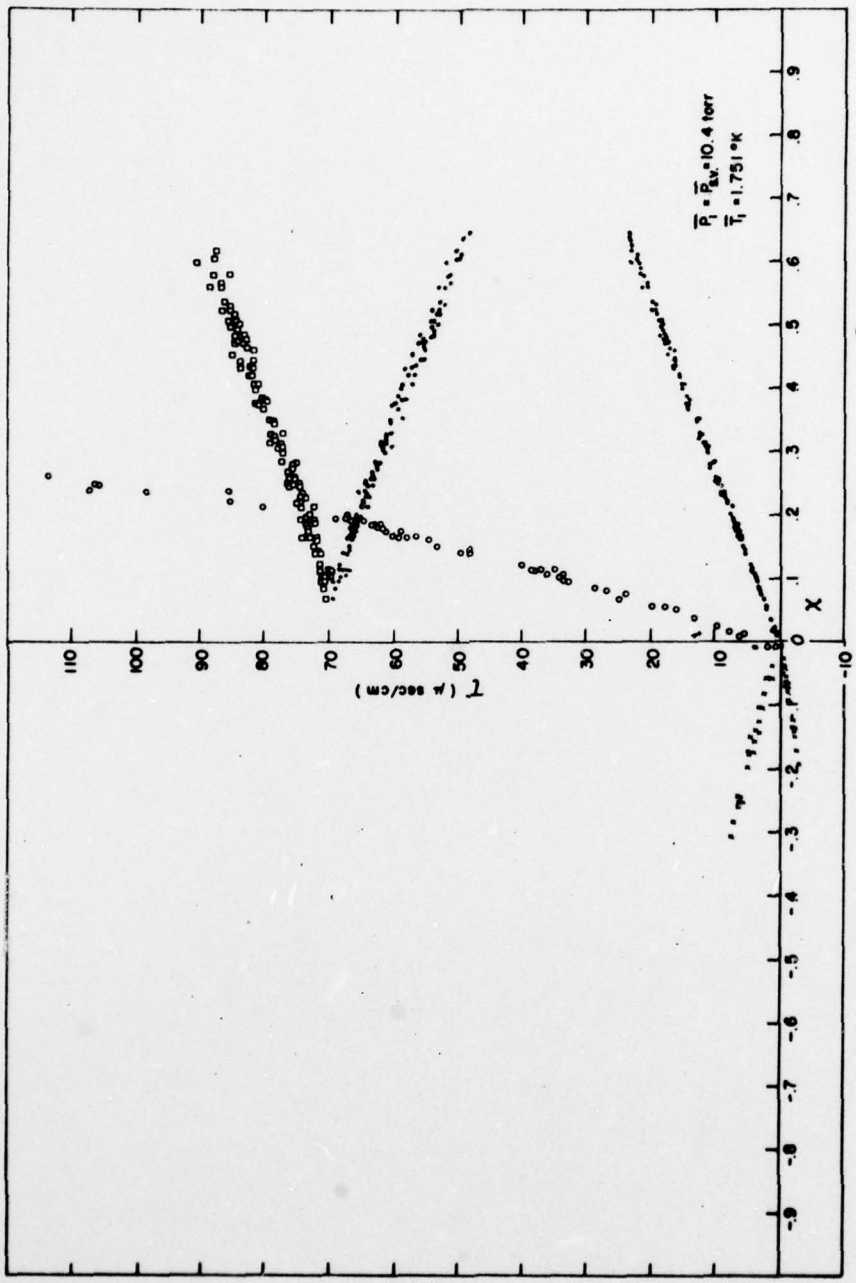

Figure 9: χ - τ Diagram for $\bar{T}_1 = 1.751^{\circ}K$

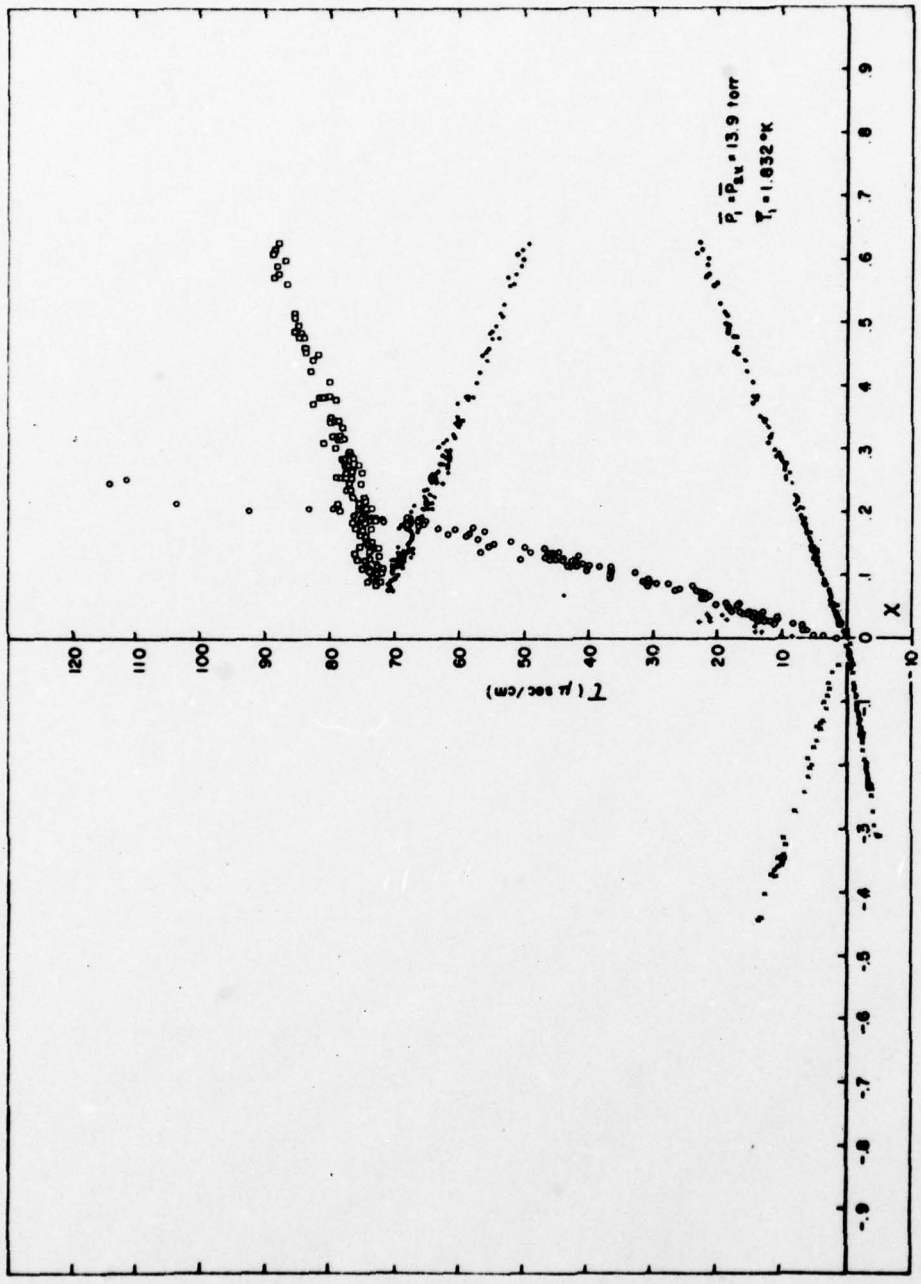

Figure 10: X - τ Diagram for $\bar{T}_1 = 1.832^{\circ}K$

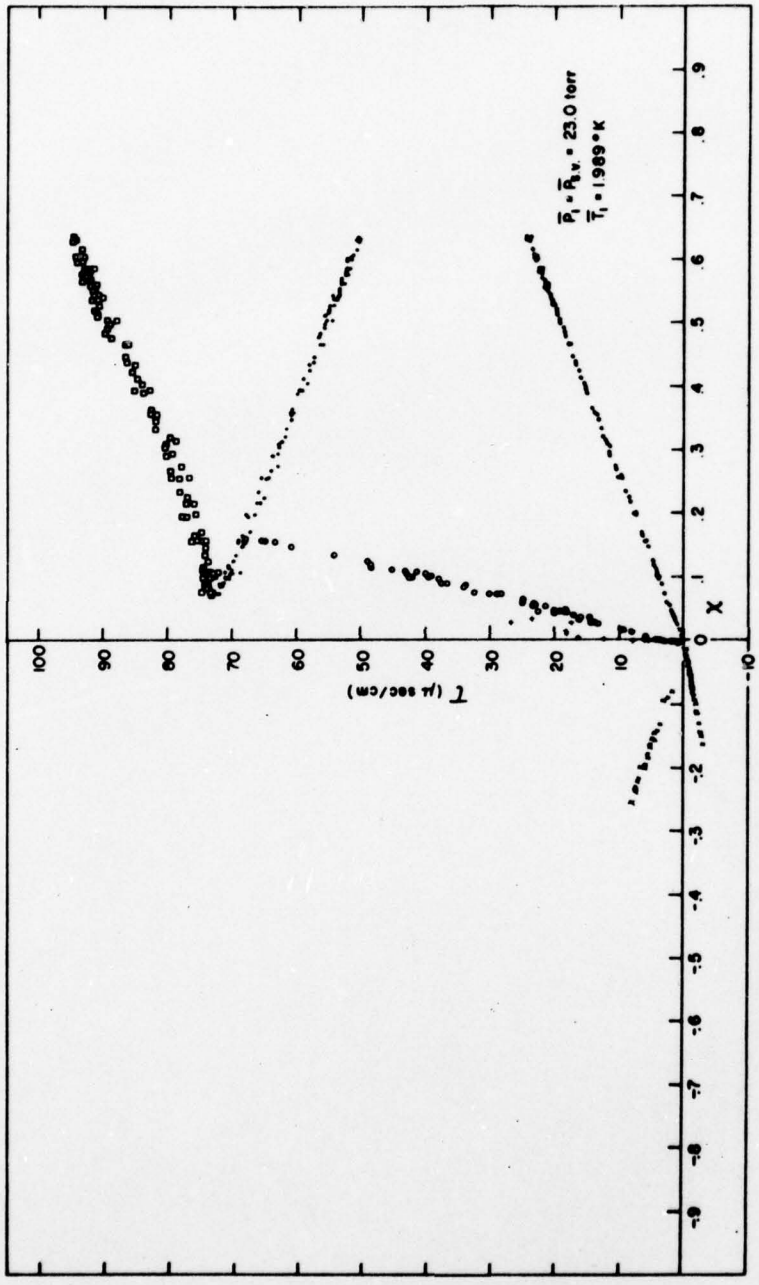

Figure 11: $\chi - \tau$ Diagram for $\bar{T}_1 = 1.989^{\circ}K$

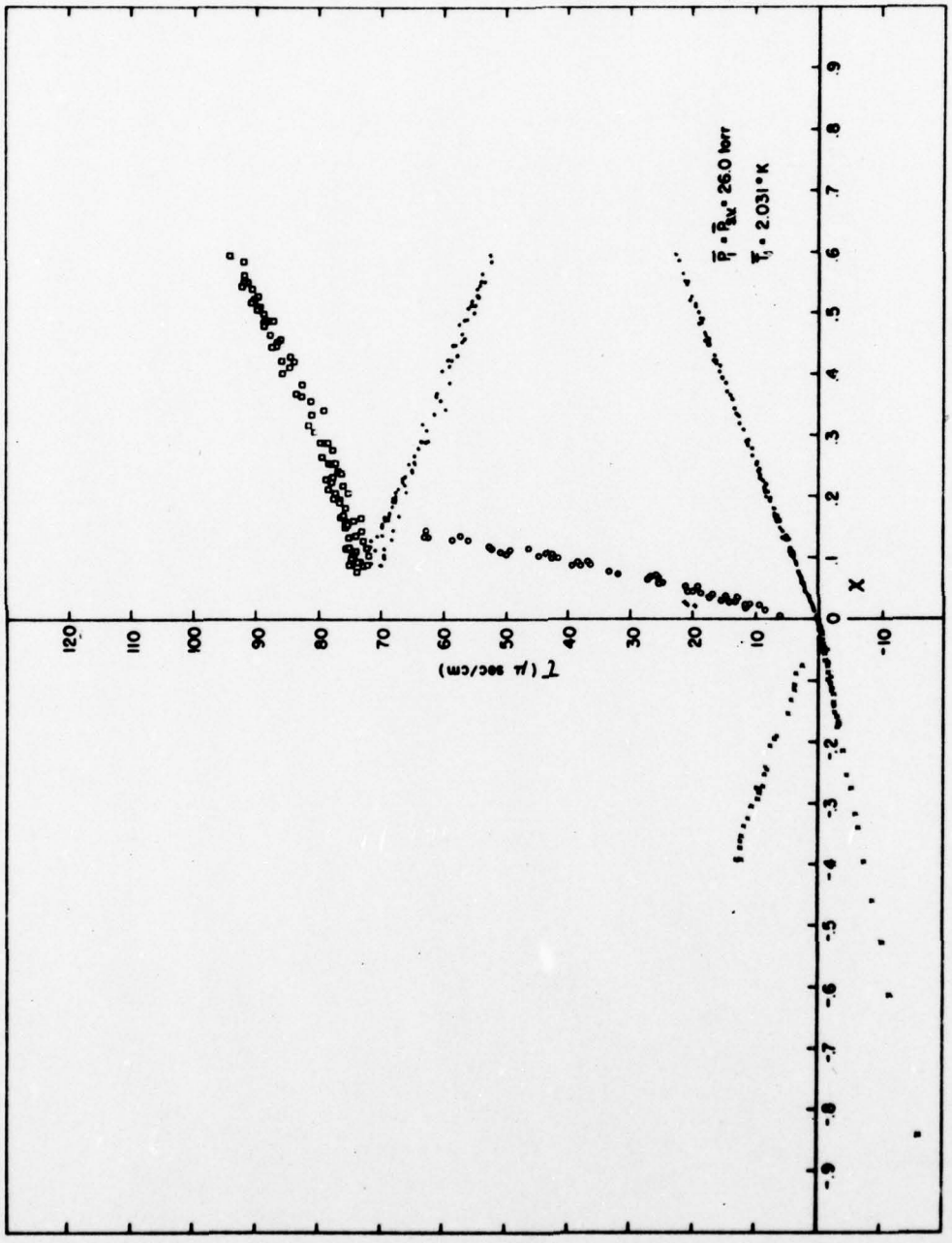

Figure 12: $\chi - \tau$ Diagram for $\bar{T}_1 = 2.031^{o}K$

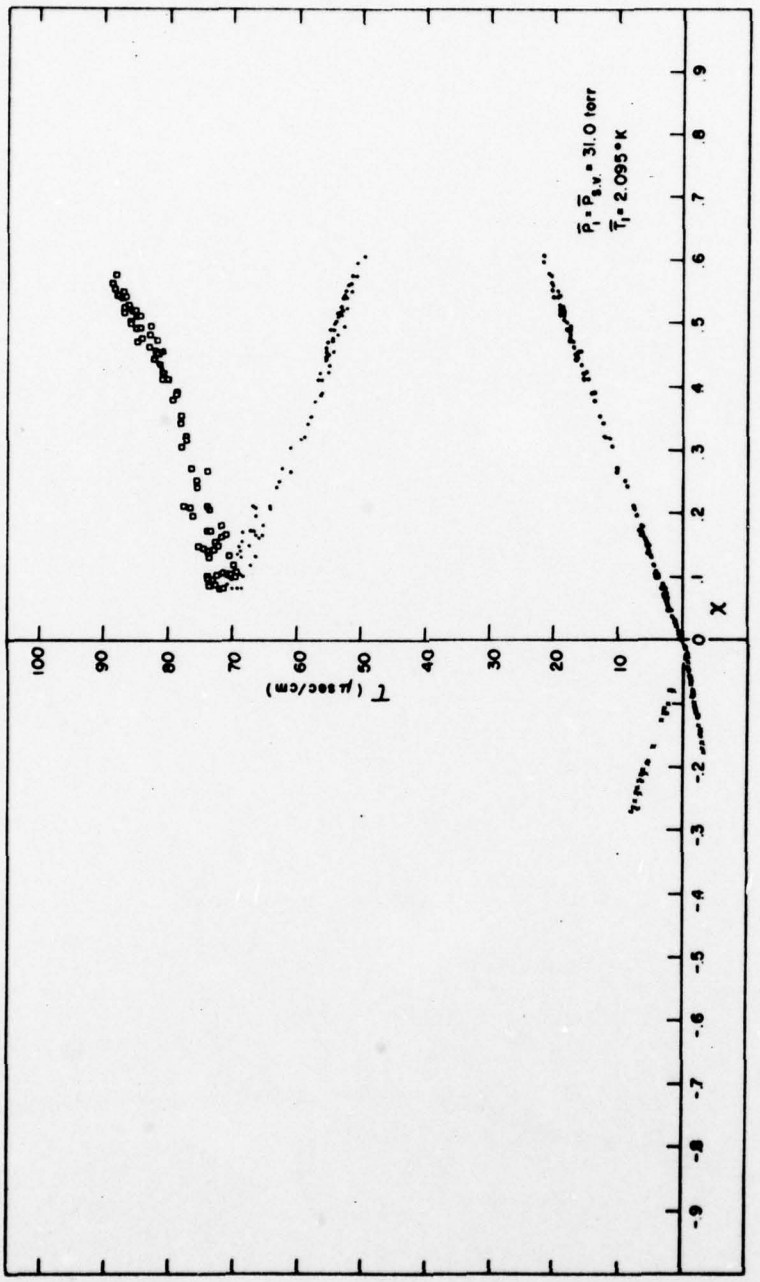

Figure 13: X - τ Diagram for $\bar{T}_1 = 2.095^{o}K$

COMPARISON OF THEORETICAL & EXPERIMENTAL VELOCITIES

Velocity	$\frac{(\ )_{exp't}}{(\ )_{theory}}$						
	1.522°K	1.665°K	1.751°K	1.832°K	1.989°K	2.031°K	2.095°K
$c_1(0)$	.99	.98	.99	.99	.96	.95	.96
$c_1(6)$	.88	.91	.86	.77	.80	.79	.71
$c_2(6)$	.90	.82	.84	.80	.77	.76	---
$u_5 = u_6$	.66	.57	.70	.51	.49	.52	.42

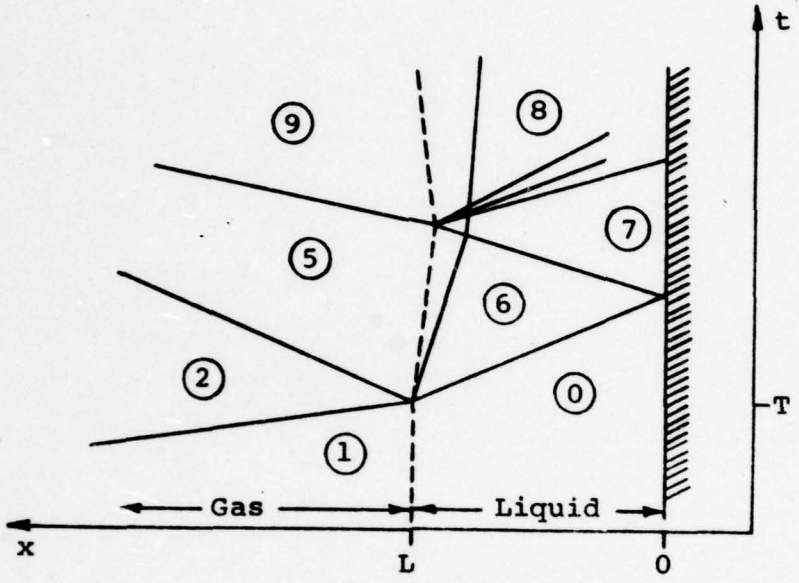

Figure 14

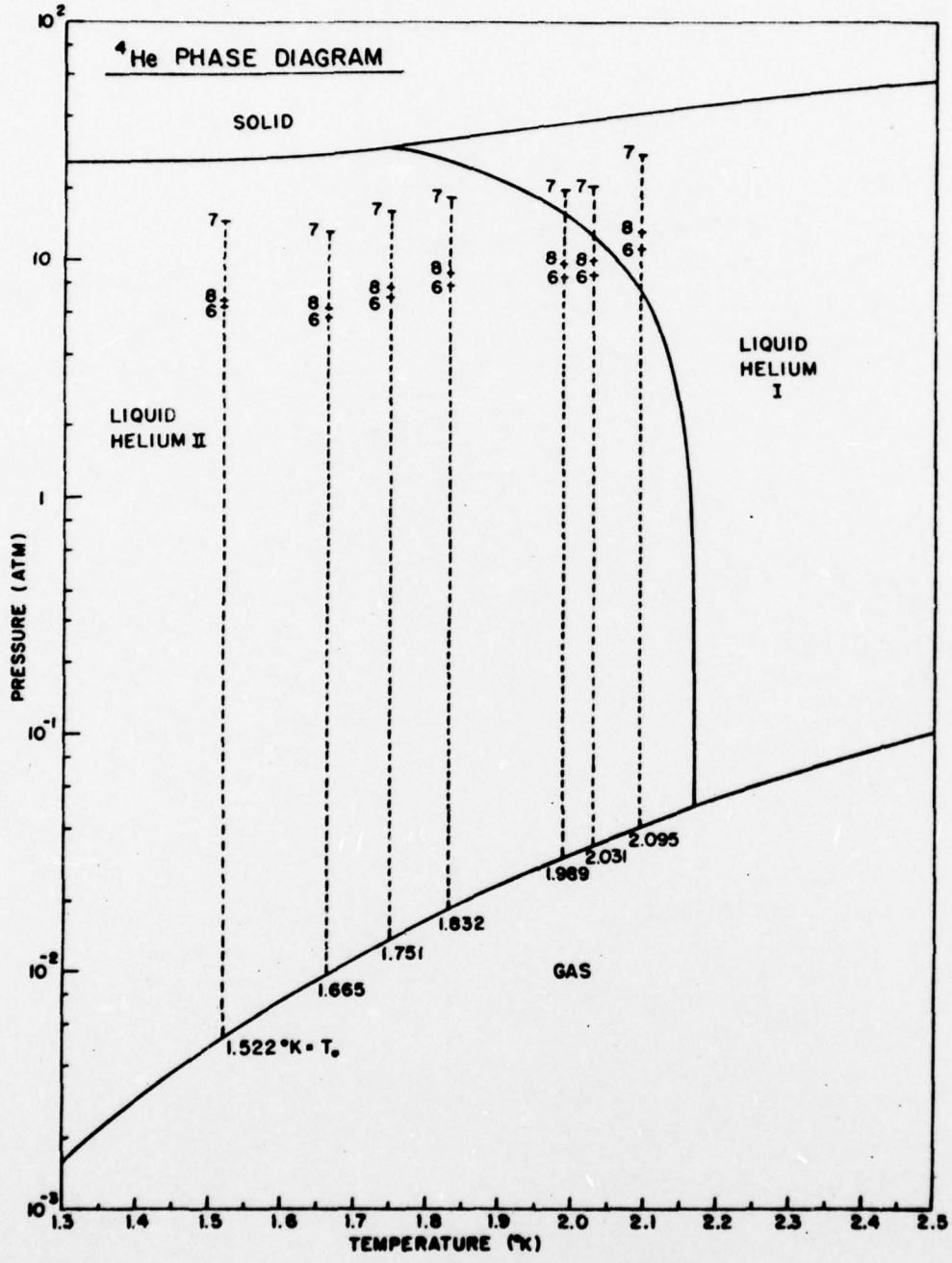

Figure 15: ^{4}He Phase Diagram

SECTION C

Experimental Investigation of Second-Sound *Shock Waves in Liquid Helium II*

Section C

LIST OF SYMBOLS

C_{1o}	first sound speed
C_{2o}	second sound speed
C_p	specific heat at constant pressure
C_v	specific heat at constant volume
M	Mach number
p	pressure
$\dot{Q}$	heat flux
s	specific entropy
T	temperature
v	bulk fluid velocity
v_n	normal fluid velocity
v_s	superfluid velocity
w	relative velocity
ℓ	shock thickness
ρ	mass density
μ	chemical potential
$( )_n$	normal fluid
$( )_s$	super fluid

I. INTRODUCTION

Background

Liquid helium, when cooled below 2.17° K, experiences a so-called λ-transition from liquid helium I to liquid helium II. Helium I behaves as a classical fluid; however, helium II exhibits non-classical behavior which can only be explained by using the concepts of quantum mechanics.

Below the λ-point, liquid helium behaves as if it were composed of two interpenetrating, noninteracting fluids: superfluid carrying no entropy and having no viscosity and normal fluid having entropy and viscosity. This two-fluid model has been used to explain many of the anomalous properties of liquid helium II.

From this two-fluid model, one can deduce two distinct forms of wave motion. When the two fluids move in phase, an ordinary pressure or sound wave is produced. However, when the two fluids move out of phase, a temperature wave, termed "second sound", is transmitted and is unique to liquid helium II. As with ordinary pressure waves, the temperature waves are non-linear in that their propagation speeds are not, in general, equal to their acoustic speeds. Hence finite amplitude perturbations can steepen to form shock waves.

The importance of these temperature waves can best be realized by a consideration of heat transfer by the liquid helium. Liquid helium II exhibits the ability of transferring large amounts of heat at practically zero temperature gradient. This phenomenon,

which is very much like that of an ordinary heat pipe, is of great importance in the cooling of superconducting magnets and other devices. However, it has been found that for heat fluxes beyond a critical value, this "supra heat conduction" breaks down, for which an adequate explanation and description does not yet exist.

Much work has been done, both experimentally and analytically, in investigating second sound waves. In particular, second sound shock waves were first observed by Osborne (1) in 1950. Later, Dessler and Fairbank (2) in 1956 studied the amplitude dependence of the second sound velocity by using a small amplitude marker pulse, first alone, and then superimposed on a larger amplitude carrier wave and comparing the times of flight.

Several optical investigations have been carried out. In 1967, Coulter, Leonard and Pike (3) used focussed shadowgraph and schlieren techniques to study the heat transport from a wire to helium II and were able, although with very poor resolution, to see second sound waves. More recently, Gulyaev (4, 5) in 1969 and 1970 optically studied large amplitude second sound using a schlieren system and constantan ribbons spaced 1 mm apart.

Cummings (6) in 1975 and later Cummings et al. (7) in 1977 studied both first sound (pressure) and second sound shock waves in helium II by using a specially constructed cryogenic shock tube to generate both pressure and temperature shocks and then later by electrically pulsing a heater and measuring the time of flight of the temperature shock waves produced.

The present investigation is an attempt to extend these results

with special emphasis on studying the critical breakdown of the superfluid heat conduction properties.

Theoretical Formulation

To develop the hydrodynamic equations of liquid helium II, we will follow Landau (8, 9) and consider the liquid helium II as composed of two fluids, the superfluid (denoted by subscript s) and the normal fluid (subscript n). We assume that the density of the liquid helium can be written as the sum of the superfluid density and the normal fluid density

$$\rho = \rho_s + \rho_n \ .$$

Also, the momentum density can be written as the sum of the superfluid and normal fluid momentum densities

$$\vec{j} = \rho\vec{v} = \rho_s\vec{v}_s + \rho_n\vec{v}_n \ .$$

Then, neglecting dissipative processes, the two-fluid conservation equations of mass, momentum and entropy can be written in the usual way

$$\text{MASS} \qquad \frac{\partial \rho}{\partial t} + \vec{\nabla}\ \vec{j} = 0$$

$$\text{MOMENTUM} \qquad \frac{\partial \vec{j}}{\partial t} + \vec{\nabla} \cdot \vec{\vec{\pi}} = 0$$

$$\text{ENTROPY} \qquad \frac{\partial \rho s}{\partial t} + \vec{\nabla} \cdot (\rho s \vec{v}_n) = 0$$

where $\vec{\vec{\pi}} = \rho_s \vec{v}_s \vec{v}_s + \rho_n \vec{v}_n \vec{v}_n + p\vec{\vec{I}}$

and $\vec{\vec{I}}$ is the identity tensor.

Two more equations are necessary to close the system. Hence, along with an equation of state, we may write an equation of motion for the superfluid alone. Since the superfluid is an ideal, irrotational fluid, we may write

$$\vec{\nabla} \times \vec{v}_s = 0 \ .$$

Consequently, $\vec{v}_s$ is the gradient of a scalar potential, and this potential can be identified as the chemical potential per unit mass, μ. Then the superfluid equation of motion can be written as

SUPERFLUID MOTION

$$\frac{\partial \vec{v}_s}{\partial t} + \vec{\nabla}\left(\tfrac{1}{2} v_s^2 + \mu\right) = 0 \ .$$

The boundary conditions at a solid surface require that the tangential component of $\vec{v}_n$ vanish from the no-slip condition, the normal component of the mass flux $\vec{j}$ vanish since there can be no mass flux through the surface, and the normal component of heat flux $\vec{q} = \rho s T \vec{v}_n$ be continuous. The set of equations, together with the boundary conditions, constitute the two-fluid hydrodynamic model for liquid helium II.

In order to extract the acoustic speeds for first and second sound, we linearize the hydrodynamic equations. With $\vec{w}$ denoting the relative velocity between the normal fluid and superfluid, $\vec{w} = \vec{v}_n - \vec{v}_s$, the linearization is performed by assuming that $\vec{v}$ and $\vec{w}$ are small, and considering small perturbations in ρ, p, T, and s about their equilibrium values. The linearized equations

can then be written

$$\frac{\partial \rho}{\partial t} + \vec{\nabla} \cdot \vec{j} = 0$$

$$\frac{\partial \vec{j}}{\partial t} + \vec{\nabla} p = 0$$

$$\frac{\partial \rho s}{\partial t} + \rho s \vec{\nabla} \cdot \vec{v}_n = 0$$

$$\frac{\partial \vec{v}_s}{\partial t} + \vec{\nabla} \mu = 0 \ .$$

These four equations can be reduced to two wave equations by using thermodynamic identities for μ and p, and

$$\frac{\partial^2 \rho}{\partial t^2} = \nabla^2 p$$

$$\frac{\partial^2 s}{\partial t^2} = \left(\frac{\rho_s}{\rho_n}\right) s^2 \quad \nabla^2 T \ .$$

By assuming fluctuations proportional to $e^{-i\omega(t - x/C)}$ where C is a wave speed, the equations can be reduced to

$$C^4 - C^2 \left[\left(\frac{\partial p}{\partial \rho}\right)_s + \frac{\rho_s}{\rho_n} \frac{T s^2}{C_v} \right] + \frac{\rho_s}{\rho_n} \frac{T s^2}{C_v} \left(\frac{\partial p}{\partial \rho}\right)_T = 0$$

which has solutions, with $\left(\frac{\partial p}{\partial \rho}\right)_s \doteq \left(\frac{\partial p}{\partial \rho}\right)_T$ from $Cp \doteq C_v$ for liquid helium II,

$$C_{10}^2 = \left(\frac{\partial p}{\partial \rho}\right)$$

$$C_{20}^2 = \frac{\rho_s}{\rho_n} \frac{T s^2}{C_p}$$

The first is the familiar sound speed while the second is the second sound acoustic speed. For first sound, the density or pressure fluctuations can be seen to be first order and $\vec{v}_s \doteq \vec{v}_n \doteq \vec{v}$: the entire liquid moves as a whole; while for second sound the entropy or temperature fluctuations are first order and $\vec{j}$ and $\vec{v}$ are approximately zero : the two fluids (normal and super) move in opposite directions.

Khalatnikov (10) determined the governing equations and jump conditions for both first and second sound shock waves by expanding the thermodynamic variables ρ, s, and μ in terms of p, T, and the relative velocity w, and retaining terms of order w^2. For temperature discontinuities, Khalatnikov found that the second sound shock speed C_2 can be expressed as

$$C_2 = C_{20} \left[1 + \frac{\Delta T}{2} \frac{\partial}{\partial T} \ln \left(C_{20}^3 \frac{\partial s}{\partial T} \right) \right]$$

and

$$w = \left(\frac{\rho}{\rho_n} \frac{s}{C_{20}} \right) \Delta T \ .$$

Recall that C_{20} is the second sound acoustic speed and was found to be

$$C_{20} = \left(\frac{\rho_s}{\rho_n} \frac{T s^2}{C_p} \right)^{\frac{1}{2}} .$$

The non-linearity of the second-sound wave can easily be seen from the expression for C_2 since the wave speed depends on the temperature jump ΔT. Note that the coefficient of the ΔT term changes its sign for $1.87^\circ K < T < 2.17^\circ K$ and hence it is possible for a negative ΔT to propagate as a shock wave in this temperature range.

The heat flux in the second sound wave, as stated above, can be expressed as

$$\dot{Q} = \rho s T v_n .$$

From the definition of the relative velocity $\vec{w} = \vec{v}_n - \vec{v}_s$ and $\vec{j} = \rho \vec{v} = \rho_s \vec{v}_s + \rho_n \vec{v}_n = 0$ for pure counterflow (as is the case for second-sound waves; i.e., no net mass flow), the heat flux can be written in terms of w:

$$\dot{Q} = \rho_s s T w .$$

Hence a critical heat flux implies a critical relative velocity and vice versa.

In an attempt to explain the sudden appearance of this critical heat flux, Gorter and Mellink (11) postulated a mutual friction mechanism between the super and normal fluids with a friction force proportional to w^3 and appended such a term to the hydrodynamic equations. Many measurements have been made of this critical

counterflow, all done in narrow channels with steady flow. In an attempt to correlate these previous measurements, Dimotakis (12) derived a relatively simple similarity law from a dimensional consideration of the hydrodynamic equations with the mutual friction terms added. For steady flow in channels, this law implies a critical value for the counterflow velocity w_c and hence for the critical heat flux $\dot{Q}_c$ as

$$w_c d \doteq \frac{1}{\pi \rho_s A}$$

where d is the diameter of the tube and A is the coefficient in the Gorter-Mellink term, given by the empirical formula (13)

$$\log_{10} A(T) = 1.10 + 3.12 \log_{10} T + \frac{0.0076}{1 - T/T_\lambda} .$$

The aims of this investigation, then, are to quantify, with experimental data, the non-linearity of the second sound shock speed and to study the critical heat flux phenomenon discussed above. Second sound shock waves are ideal for this purpose as the shock speed (and hence amplitude) is dependent on the heat input. Consequently, for a known heat input pulse, a measurable and repeatable wave is produced. Since all previous measurements of critical counterflow have been done with steady flow, an investigation can be made into the effects of nonsteady heat transfer (using these temperature shock waves) on the critical counterflow velocity. These results can then be used to determine the validity of the Dimotakis

similarity law in nonsteady flow.

II. EXPERIMENTAL APPARATUS

Shock Tube

The method chosen as the most practical for producing the second sound shock waves consisted of electrically pulsing a suitable heating element and following the wave thus produced as it travels along a tube. Since, from the two-fluid model, heat is convected away by the normal fluid, and the total mass flux in the tube is zero, a counterflow is set up when the heating element is pulsed, creating a temperature wave.

The "second sound shock tube" designed and constructed for this investigation consists of a one inch square cross section Plexiglas tube with provisions for a heater at one end and temperature detectors at the opposite end and also along one sidewall. The shock tube is shown in Figure 1. The heater mounts on the flange at the bottom and sealing is attempted using a silicon rubber "gasket". Detectors, which will be discussed below, can be mounted on the top of the four inch long tube, for endwall measurements, and also along the removable sidewall by spring clamping a glass sensor slide in place. Since all structural parts are constructed from Plexiglas, there can be no differential shrinkage and hence all angular alignments are maintained when the shock tube is cooled to liquid helium temperatures. The entire shock tube assembly is immersed in liquid helium and since it is not completely sealed, the liquid helium can fill the tube. All work is done at the saturated vapor pressure with the height of liquid above

the tube providing enough hydrostatic pressure above SVP to allow the firing of at least smaller heat pulses without significant boiling.

Heater

Several considerations affected the design of the heating element used to produce the second sound shock waves. First, the element should be capable of withstanding large voltage pulses, on the order of 100 - 200 volts. Second, the heater must have a very fast time response in order to closely follow the shape of the voltage input. Finally, the heater assembly must be able to survive repeated cycling to liquid helium temperatures.

In order to get the necessary time response, it was decided to use a thin film element as the heater. After much experimentation with different substances, it was found that Nichrome, vacuum evaporated onto a quartz substrate to a thickness of approximately 1000 angstroms, gave the best results in terms of film electrical resistance (the order of 10 ohms) and durability. Quartz was chosen as a substrate for its good thermal properties, especially its strength when cooled to liquid helium temperatures.

Electrical contact to the heater film was accomplished by evaporating 1000 Å thick copper pads at the edges of the Nichrome film and attaching the input wire leads by mechanical clamps, using coiled indium wire between the clamp and the evaporated copper pad. This method of attaching the leads proved very satisfactory and gave no major problems. Sufficient force could be applied to compress the indium wire to insure electrical contact

when cooled to liquid helium temperatures. A photograph of a typical heater appears in Figure 2.

The electrical heater pulse is created by a specially designed pulser, capable of generating pulses of up to 100 volts amplitude and duration ranging from several microseconds to over 10 milliseconds. Furthermore, the high voltage pulser can follow any input waveform, in order to see the effects of a slowly rising heat pulse on the shock wave produced. An oscilloscope trace of a typical voltage pulse is shown in Figure 3.

Detectors

In order to measure the temperature amplitudes of the second sound shock waves, it was decided to follow an earlier development by Laguna (14) and use superconducting thin films with adjustable transition temperatures. Different superconducting materials and techniques were tried with varied success, including tantalum on titanium, aluminum oxide, and tin on gold, all deposited on various substrates. The tantalum on titanium deposited on silicon proved to be the most durable, and after repeated cycling in liquid helium, showed no sign of degradation. However, the final detectors used, which gave the best results, were gold evaporated on tin, deposited on a quartz or pyrex glass substrate. The reasons for choosing the tin-gold film will be discussed below. Pure tin is vacuum evaporated to form a film 1000 Å thick. Then 250 Å of gold is deposited on the tin and the combination is then photo-etched following a technique used by Laguna (14) to form the actual detector. The detector

consists of a strip of this gold-tin combination, 0.025 mm wide and 10 mm long, with pure tin superconducting leads to make connections to the lead-in cables. These connections are made with pressed indium. A photograph of a typical detector slide is shown in Figure 4. The basic transition temperature of these superconducting thin films is determined by the ratio of gold to tin (pure tin transitions at 3.74° K); however, the transition temperature can be lowered by applying a magnetic field to the film, and by this means the transition temperature can be set to whatever point is desired. The temperature variations due to the passage of the second sound wave cause changes in the film resistance, and with a constant bias current, changes in the voltage drop across it. By adjusting the magnetic field so as to have the film transition to its superconducting state at the working shock tube temperature, as shown in Figure 5, a large slope, $\frac{dV}{dT}$, of voltage drop versus temperature and therefore a large sensitivity, can be obtained. The detectors are calibrated under static conditions by recording the voltage drop across the film for a fixed magnetic field as the bath temperature is slowly varied.

The signal from the detector is then amplified by an ultra low-noise preamplifier (Princeton Applied Research Model 113), and a voltage-time history of the second sound shock passage is recorded on an oscilloscope.

Data Reduction Technique

In order to obtain the second sound shock speed, a digital

interval counter (Hewlett-Packard Model 5326B Counter-Timer DVM) with a resolution of 0.1 μsec., is used to measure the time of flight of the wave, either from the heater to the detector, or between two detectors. For the heater to detector case, the counter is triggered on by the voltage pulse into the heater and off by the sensor output. In the detector to detector case the counter measures the time of flight of the wave between two detectors a known distance apart.

Temperature amplitude information can be obtained from the detector voltage-time history recorded on an oscilloscope. The voltage to temperature conversion is determined from the static calibration curves for each sensor, and knowing the amplifier gain, the temperature jump, ΔT, can be determined by measuring the voltage amplitudes from the oscilloscope traces. In this manner, plots of shock strength $\frac{\Delta T}{T}$, versus shock "Mach number" (wave speed divided by the local second sound acoustic speed) and also heater input power versus Mach number can be obtained.

III. RESULTS

The quality of the signal produced from the superconducting detectors is demonstrated in Figure 6. It shows the response of a tin on gold sidewall detector to a heat pulse propagating through the liquid. The wave is travelling from right to left in the photograph and the second sound shock can clearly be seen to be at the front of the pulse. The heat pulse in Figure 6 was generated from a square voltage pulse, similar to the one shown in Figure 3, however of 100 μsec duration. From the fast risetime of the shock (the risetime measured from the photograph is limited by the amplifier bandwidth, the actual risetime is much less than a microsecond) and the low noise level of the signal, very accurate measurements of the wave speed can be made.

Figure 7 shows a series of heat pulses, all produced by rectangular voltage pulses, and it can readily be seen how the heat pulse shape develops as it propagates along the tube. In exact analogy with corresponding piston produced pressure shock waves in gases, it is evident that the trailing edge of the pulse catches up to the shock front. One interesting feature to note in these oscilloscope traces are the small pulses following behind the heat pulse. These "blips" appear in all traces and can be seen to overtake the heat pulse and eventually ride on top of it. These pulses will be discussed in greater detail later on.

Also in analogy with ordinary pressure sound waves, the second sound shock waves reflect from an endwall with a cor-

responding doubling of the amplitude. Figure 8 shows heat pulses reflecting from a solid endwall. The detectors in these photographs are tin on gold sidewall detectors and the upper trace in each oscillograph is a sidewall detector closest to the heater, while the lower trace is one closest to the endwall. Figure 8a shows the reflection of a 10 msec long heat pulse while Figure 8b shows 100 μsec pulses. As before, wave propagation is to the left and the incident wave (on the left) and the reflected wave (on the right) are both clearly visible. The temperature amplitude doubling is readily seen in Figure 8a.

Also apparent in both photographs are the "blips" mentioned above, and the existence of both positive and negative "blips" is clearly evident.

Figure 9 shows oscilloscope traces of heat pulses of various lengths from 250 μsec to 10 msec. There seems to be no qualitative difference in pulse shape from short pulses to long ones except that the trailing edge never overtakes the shock front in the very long pulses, at least in the length of the shock tube.

A superconducting detector was mounted on the end of a probe installed in the center of the shock tube in order to investigate any difference in waveform that may exist between the center and sidewall of the shock tube. Oscilloscope traces of the detector output are shown in Figure 10. The lower traces are the center probe outputs while the upper traces are the sidewall detector outputs. Figure 10a shows 100 μsec long heat pulses and Figure 10b shows

10 msec pulses. In Figure 10b there appears a significant difference between the center and sidewall traces. While this difference is also seen in Figure 10a, the effect is more easily explainable using the longer pulses shown in Figure 10b. Referring to Figure 10c, we note the wave shape: after passage of the shock front, the pulse stays flat for a time of 0.0205 msec corresponding to a length of 0.42 mm (using the second sound acoustic speed $C_{20} = 20.41$ m/sec for a bath temperature of 1.65° K) or one-half the width of the center probe end. The temperature amplitude decays to one-half the initial amplitude (height h in the drawing) in 0.089 msec corresponding to a distance of 1.817 mm or one-half the length of the sensor strip. From the data collected in endwall measurements, it was found that an end-mounted detector output is twice the amplitude of the incident wave, as was seen from an examination of the reflected wave traces in Figure 8. However, due to the fact that the detector does not occupy the entire area of the shock tube, diffracted waves will be generated at the edges of the detector as the shock front passes, as shown in Figure 10c. These waves cause the amplitude of the reflected wave measured by the end-mounted probe to decay until the amplitude is that of the incident wave. This is the behavior clearly seen in Figure 10b.

As mentioned earlier, a series of alternating positive and negative pulses appears following every heat pulse. Although no conclusive evidence has as yet been obtained, results thus far lead to several possible explanations as to their origin. Perhaps the most plausible origin of these pulses is possible diffracted

waves generated at the edges of the thin film heater, where the shock tube joins the substrate. Although the wavelength of the "blips" and the spacing between the ones in the series do not exactly match the expected values for diffraction waves, the numbers are close enough so as to not be discounted. Attempts were made to seal the joint between the heater film and shock tube; however, it could not be determined if the joint was properly sealed against a "superleak", and since the pulses still appeared, no conclusive results were obtained. The small pulses are definitely not generated by the heater, as there is no possible way to generate a negative temperature wave (below ambient temperature) using an electrically-excited heater. As can be seen from an examination of the heater voltage pulse, shown in Figure 3, there is no evidence of any extraneous pulses which could be causing these "blips". One other possible explanation is the small pulses are evidence of some sort of motion left behind in the wake of the heat pulse, possibly indicative of vortices generated by the passage of the second sound shock pulse. More work needs to be done in order to be conclusive as to the origin of these pulses.

Figures 11 - 14 show plots of shock strength, $\frac{\Delta T}{T}$, versus the ratio of shock wave speed to second sound speed (called "Mach number" in analogy with ordinary gasdynamic shocks) for various detectors and detector locations. Figures 11 and 12 are for end mounted detectors, Figure 11 showing the results obtained from an endwall mounted tantalum-on-titanium detector and Figure 12 showing an endwall tin-on-gold detector along with the results from

the center-probe, also an end mounted tin-on-gold detector. While the qualitative shape of both plots is essentially the same, the shock amplitudes given by the tin-gold detectors are much higher than those from the tantalum. This discrepancy can be explained by considering the composition and construction of the two types of detectors.

The tantalum-titanium detector is fabricated by depositing tantalum on top of titanium which had been deposited on a silicon substrate. The tantalum is then anodized to a certain depth to produce a superconducting transition temperature in the desired range. This produces an oxide layer on top of the actual superconducting detector strip which acts as a thermal insulator for the detector. Hence the detector cannot measure the full temperature jump produced by the shock. In addition, the silicon substrate is an excellent heat conductor, which enhances this problem. To verify this, a tantalum-titanium detector was fabricated on a glass substrate which resulted in significantly higher amplitudes.

Plotted in Figure 12 are data from several different experimental runs as shown, and for three heat pulse lengths: 100 μsec, 3 msec, and 10 msec. As can be seen from the data, there appears to be no appreciable difference in the behavior of the shock wave for the range of pulse lengths used in the initial linear region of the plot. However, the data seem to indicate that the shorter, 100 μsec, pulses were capable of reaching a higher temperature amplitude than the longer pulses. Although more data

need to be obtained, other experimental runs seem to support this observation.

The development of a critical limit of shock strength in the region $1.04 \leq M < 1.06$ is clearly evident in both figures. This behavior will be discussed in greater detail below.

Figure 13 shows a plot of shock strength versus Mach number for a sidewall-mounted tin on gold detector for two different experimental runs. Again the development of this critical limit in shock strength is evident. Note that the temperature amplitudes shown here are one-half those of the endwall measurements, as is expected. Also shown for comparison is a calculation of the shock strength versus Mach number as given by Khalatnikov (10) and developed above. Recall that

$$C_2 = C_{20}\left[1 + \frac{\Delta T}{2}\frac{\partial}{\partial T}\ln\left(C_{20}^3\frac{\partial s}{\partial T}\right)\right].$$

Now with $\frac{\partial s}{\partial T} = \frac{C_p}{T}$, we can write

$$M = \frac{C_2}{C_{20}} = 1 + \frac{\Delta T}{T}\left[\frac{3}{2}\frac{T}{C_{20}} + \frac{\partial C_{20}}{\partial T} + \frac{T}{2C_p}\frac{\partial C_p}{\partial T} - \frac{1}{2}\right].$$

The derivatives appearing in the brackets can be calculated by using the result from Chapter I for C_{20} and the definition of $\rho_s = \rho - \rho_n$ to give

$$C_{20}^2 = \left(\frac{\rho}{\rho_n} - 1\right)s^2\frac{T}{C_p}.$$

This gives M in terms of temperature derivatives of $\frac{\rho_n}{\rho}$ and C_p, which have been tabulated by Maynard (15). Evaluating the expression for M at the initial temperature of 1.65° K and the corresponding saturated vapor pressure, we find for M in terms of the shock strength

$$M = 1 + 1.4704 \frac{\Delta T}{T} ,$$

which is shown in Figure 13.

The discrepancy between the calculated values of $\frac{\Delta T}{T}$ and the measured values can again be explained in terms of an insulating oxide layer existing on top of the detector film.

Since the detectors are calibrated under static conditions it is not clear that the calibration is valid for the existing dynamic passage of the heat pulse, since in the static case, the film substrate has time to come to equilibrium with the liquid helium bath, while in the actual shock wave case, this certainly does not occur, and hence the film may not be responding properly to the shock amplitude. This could easily be analyzed using the heat equation; however, reliable data for the thermal conductivity and thermal diffusivity could not be found for these materials at liquid helium temperatures.

Shock wave speed, determined by measuring the time of flight between two sidewall detectors, as opposed to measuring time of flight between the heater and detector as in the previous cases, is plotted with shock strength in Figure 14. These data were obtained using gold on tin detectors in order to attempt to further reduce the oxide layer which forms on the tin due to exposure to the atmosphere.

However, due to the relatively thin (250 Å) layer of gold, and the apparent intermingling of the tin and the gold rather than a gold layer forming on top of the tin, a tin oxide layer is still definitely produced. Also, since the problem of the response of the substrate to the wave passage, as already discussed, still exists, the temperature amplitudes measured still are below the calculated values.

The qualitative appearance of the data, however, is considerably different in Figure 14 than in the previous plots. Whereas in the previous figures, the data fold over, but with an apparent increase in wave speed for the same shock strength, no such behavior is seen in Figure 14. In fact, for increasing heater power input, the shock strength increases to a maximum value, $\frac{\Delta T}{T} = 0.0197$ in Figure 14, then folds back on itself unlike the previous measurements. In order to distinguish the higher heat input data (folded portion past the critical limit) from the lower heat values, a different symbol has been used for these points. Thus, a unique shock strength implies a unique wave speed, as would be expected. One plausible explanation for the difference between the two curves (heater to detector and detector to detector measurements) is liquid helium boiling at the heater surface. For the higher amplitude pulses, the liquid helium definitely vaporizes at the heater surface (verified visually and by an audible "clicking" sound). If the wave speed is determined by measuring time of flight from the heater to detector and there is the formation of a vapor bubble, then the actual time

of flight of the wave may not be properly determined. This situation is eliminated by measuring time of flight between two detectors placed far enough downstream so that the shock wave passes by after the heater boiling has stopped. Further verification of this phenomenon is obtained using pulses of 10 msec duration. The heater boiling (i.e., the voltage pulse to the heater) has not stopped before the shock wave passes the detectors and a folding in the curve, similar to the heater to detector case, is observed.

The apparent critical limit in shock strength seen in the data presented could be attributed to liquid boiling behind the shock wave. Since the experiment is conducted at the saturated vapor pressure with only the head of liquid helium above the shock tube, calculations indicate that certain combinations of large amplitude shock waves with lower levels of liquid helium in the bath could result in boiling behind the wave. This would indicate that in order to increase the heat pulse amplitude, a pressurized system is necessary.

Another explanation for the peak in the shock strength is the reaching of the critical limit in heat flux, or counterflow velocity w, as discussed above. While the magnitude of the critical Mach number does not appear very large, the dependence of the heat flux in the wave on the counterflow velocity produced by the shock is very pronounced, as indicated in Figures 15 and 16, where heat flux is plotted against shock Mach number (and hence the counterflow velocity, w, which depends on M) for the heater to detector measurements (Figure 15) and the detector to detector measure-

ments (Figure 16). The heat fluxes plotted in these figures are calculated in the following manner :

Recall that the heat flux can be expressed as

$$\dot{Q} = \rho_s s T w .$$

From the expression for w :

$$w = \frac{\rho}{\rho_n} \frac{sT}{C_{20}} \frac{\Delta T}{T} ,$$

the heat flux can be written

$$\dot{Q} = \rho C_{20} C_p T \frac{\Delta T}{T} ,$$

or

$$\dot{Q} = \rho C_{20}^3 \left(\frac{\rho_n / \rho}{1 - \rho_n / \rho} \right) \left(\frac{C_p^2}{s^2} \right) \frac{\Delta T}{T} .$$

For $T_o = 1.65^o K$,

$$\dot{Q} = 9.1407 \times 10^6 \frac{\Delta T}{T} \quad \frac{Watts}{m^3} .$$

Since $\frac{\Delta T}{T}$ is related to the Mach number M, $\dot{Q}$ can be expressed in terms of M if desired.

Since the counterflow velocity, w, is related to the shock strength $\frac{\Delta T}{T}$, we can calculate the value of w for the critical limit of $\frac{\Delta T}{T}$ in the data. From

$$w = \left[\frac{\rho}{\rho_n} \frac{sT}{C_{20}} \right] \frac{\Delta T}{T} ,$$

we compute a $w_{max} = 2.51 \frac{m}{sec}$ for $\frac{\Delta T}{T} = 0.018$ and $T_o = 1.6420^\circ K$. This value of w_{max} is at least one order of magnitude greater than previously found for steady channel flow. If the value of w is computed using the Mach number at the observed critical point, which can be related to $\frac{\Delta T}{T}$ by Khalatnikov's theory, then a value of w = 3.77 m/sec is obtained, which is even greater than before. Hence, since the critical heat flux is related to the critical counterflow velocity, it would be expected that heat fluxes at least an order of magnitude greater can be transported using pulsed techniques.

If we assume the Dimotakis similarity is valid for this geometry, then a length scale is needed. At least close to the shock front, the critical value for the counterflow velocity cannot depend on the tube dimensions. Hence, the only apparent length scale entering the problem is the shock thickness. Provided the peak in the shock strength data is the critical condition, we can apply the Dimotakis similarity to calculate the shock thickness. Recall that the similarity parameter is expressed as

$$\rho_s A w_c \ell = \text{const} \doteq 1$$

or

$$w_c \ell = \frac{1}{\rho_s A} ,$$

where A is the Gorter-Mellink constant. Using the value of $w_{max} = w_c = 2.51$ m/sec calculated above, we arrive at a length, or shock

thickness, of $\ell = 5.42\ \mu$. Moreover, using the adjusted value of $w_{max} = 3.77$ m/sec, we compute a thickness of $3.61\ \mu$.

Figure 17 shows a plot of heater power versus shock Mach number for two different pulse lengths obtained from detector to detector measurements. It is apparent that the same peak appears in these data as in the amplitude measurements. Very similar data has been published by Cummings et al. (7) and the agreement is extremely good. They find a folding in the curve at the same heater power (about 20 - 30 Watts/cm^2) as is shown here. Note that the initial part of the curve is linear, in agreement with the theory. Also noteworthy are the apparent oscillations in the data for the 250 μsec pulses after the peak in the curve. This behavior was also seen in the data from the center probe measurements, shown in Figure 18. These oscillations can be correlated to the "blips" mentioned above catching up and overtaking the heat pulse. As the alternating positive and negative pulses overtake the heat pulse and shock front, the data undergo the oscillatory behavior shown. There are not enough data to be conclusive as to whether this effect is caused by the "blips", or both caused by a third phenomenon, or whether the correlation is merely coincidental.

IV. CONCLUSIONS

A facility to study second sound shock waves was designed and constructed. Preliminary measurements using superconducting thin film detectors indicate the existence of a critical breakdown of the "supra heat conductivity" of the liquid helium II at much higher heat fluxes than previously measured in the steady flow condition. The ability to transfer larger amounts of heat using pulsed techniques is of great technological importance. Qualitative confirmation of Khalatnikov's linear theory was accomplished, and agreement with other known results was established. Performing these measurements in a pressurized system will definitely shed more light on the question of critical breakdown, as the boiling problem encountered in this investigation will be eliminated.

REFERENCES

1. Osborne, D.V., Proc. Phys. Soc. (London) A64, 114 (1951).
2. Dessler, A.J. and Fairbank, W.M., Phys. Rev. 104, 6 (1956).
3. Coulter, D.M., Leonard, A.C. and Pike, J.G., Advances in Cryogenic Engineering, Vol. 13, Plenum Press, p. 640 (1968).
4. Gulyaev, A.I., Zh. Eksp. Teor. Fiz. 57, 59 (1969).
5. Gulyaev, A.I., Zh. Eksp. Teor. Fiz. Pis. Red. 11, 332 (1970).
6. Cummings, J.C., J. Fluid Mech. 75, 373 (1976).
7. Cummings, J.C., Schmidt, D.W. and Wagner, W.J., Phys. Fluids 21, (5), 713 (1978).
8. Landau, L., J. Phys. USSR 5, 71 (1941).
9. Landau, L.D. and Lifshitz, E.M., Fluid Mechanics, Pergamon Press (1959).
10. Khalatnikov, I.M., Introduction to the Theory of Superfluidity, translated by Pierre C. Hohenberg, W.A. Benjamin, Inc., New York (1965).
11. Gorter, C.J. and Mellink, J.H., Physica 15, 285 (1949).
12. Dimotakis, P.E., Phys. Rev. A, 10 (5) (1974).
13. Dimotakis, P.E. and Broadwell, J.E., Phys. Fluids 16, 1787, (1973).
14. Laguna, G.A., Ph.D. Thesis, California Institute of Technology (1975).
15. Maynard, J., Phys. Rev. B, 14, (9), (1976).

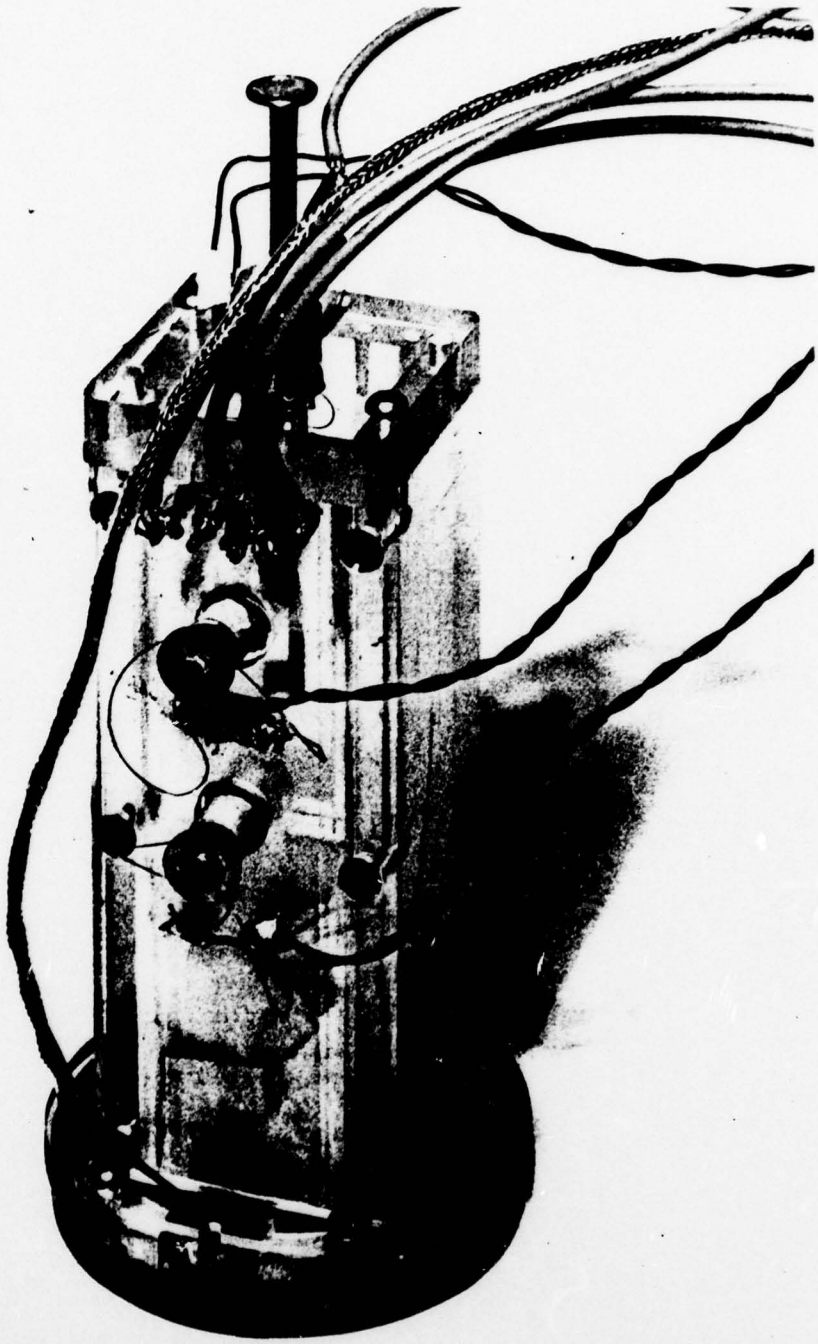

FIGURE 1 SECOND SOUND SHOCK TUBE WITH HEATER, SIDEWALL DETECTORS, AND CENTER PROBE INSTALLED

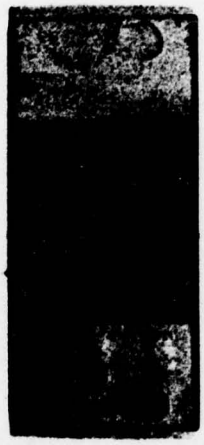

FIGURE 2 TYPICAL NICHROME HEATER WITH COPPER LEADS

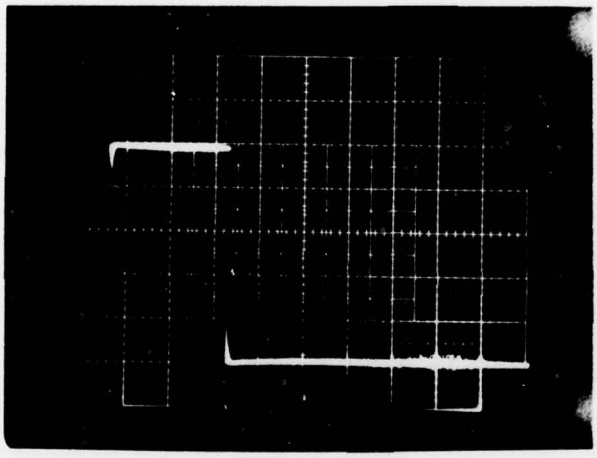

5 volt/div
0.5 m sec/div

FIGURE 3 OSCILLOSCOPE TRACE OF TYPICAL HEATER VOLTAGE PULSE

FIGURE 4 TYPICAL GOLD ON TIN SIDEWALL DETECTOR SLIDE

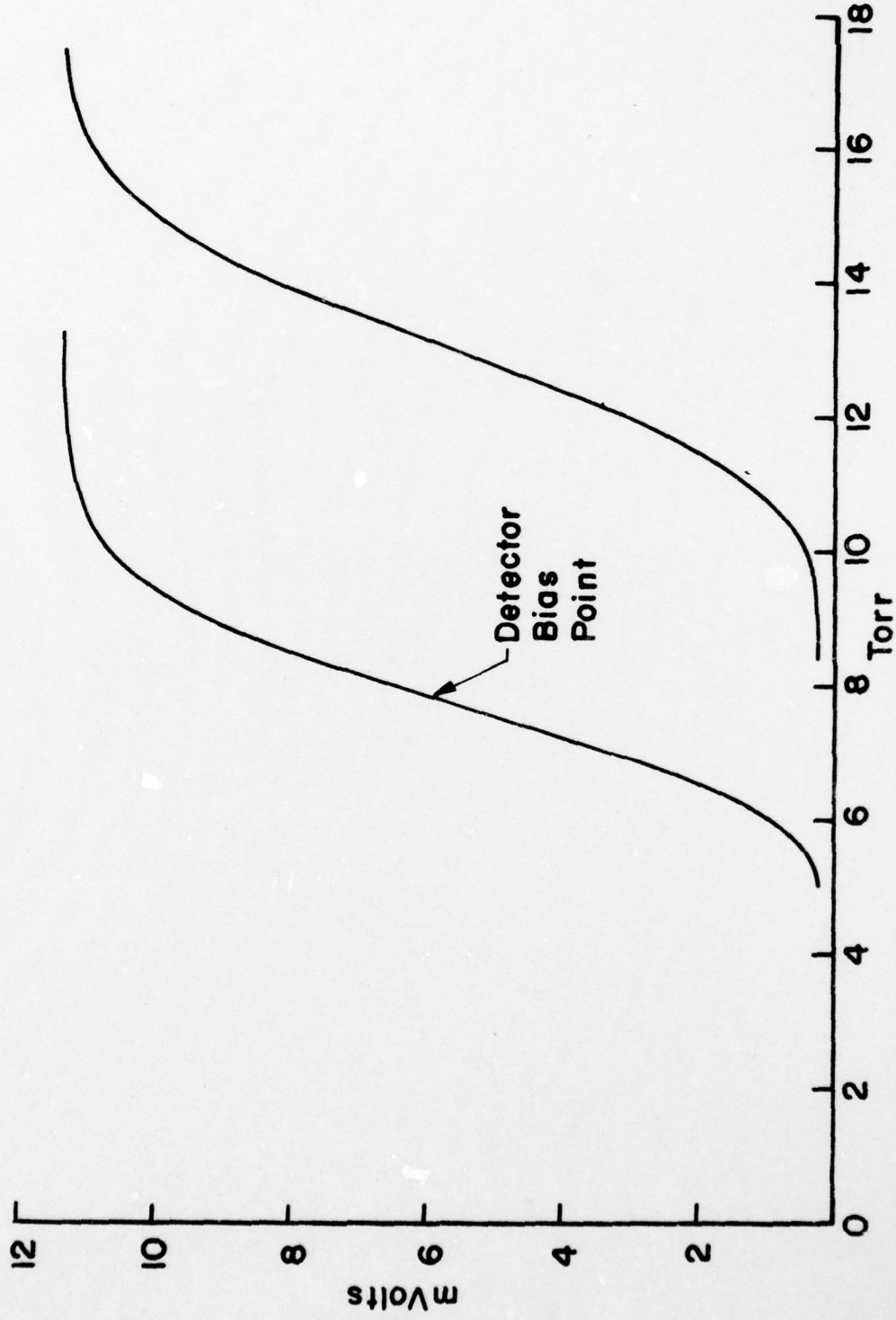

FIGURE 5 TYPICAL DETECTOR VOLTAGE BIAS CURVES FOR VARIOUS APPLIED MAGNETIC FIELDS

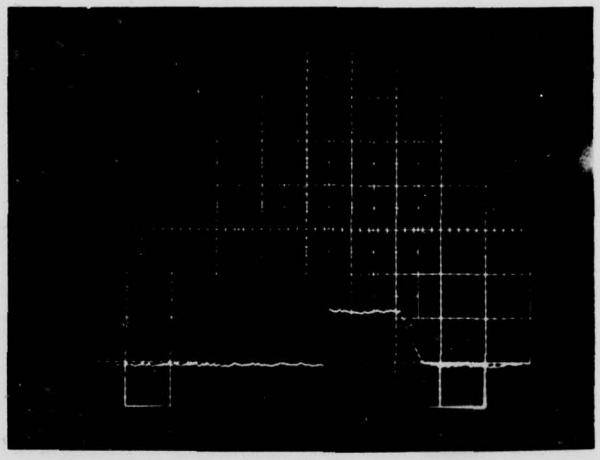

$T_o = 1.64°K$

2.35 mK/div

50 μ sec/div

FIGURE 6 TYPICAL OSCILLOSCOPE TRACE OF SECOND SOUND SHOCK WAVE AS MEASURED BY A SUPERCONDUCTING DETECTOR

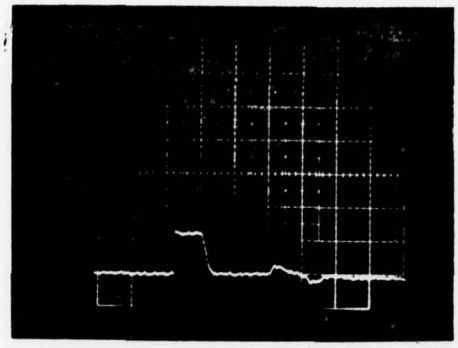

7a. 2.35 mK/div
100 μ sec/div

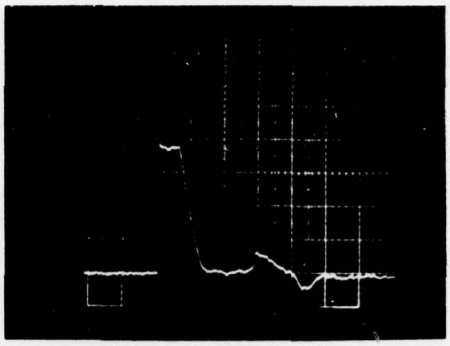

7b. 2.35 mK/div
100 μ sec/div

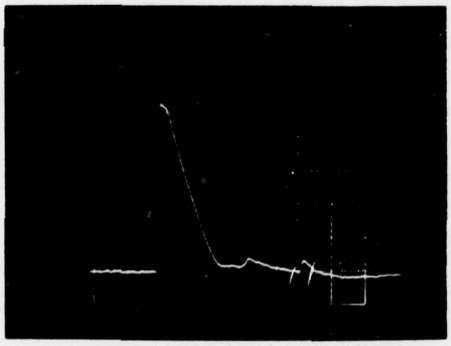

7c. 4.70 mK/div
100 μ sec/div

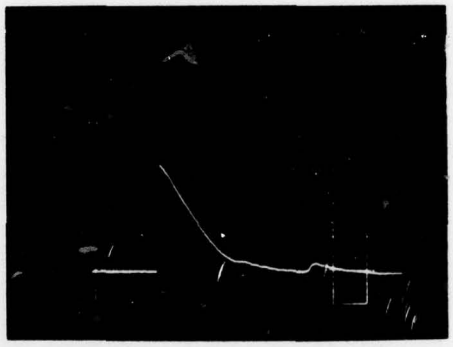

7d. 9.45 mK/div
100 μ sec/div

$T_o = 1.64°K$

FIGURE 7 TYPICAL VARIATION OF HEAT PULSE SHAPE AS TRAILING EDGE OVERTAKES SECOND SOUND SHOCK

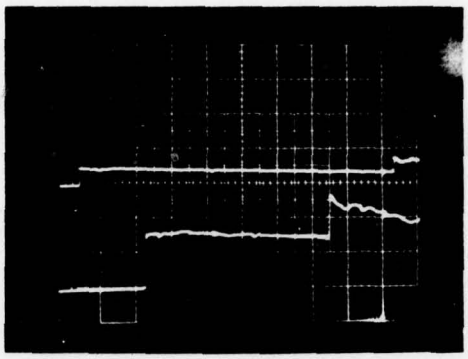

8a. upper trace: 5 m volt/div
lower trace: 500 m volt/div
horizontal: 500 μ sec/div
10 msec Heat Pulse
T_o = 1.68 °K

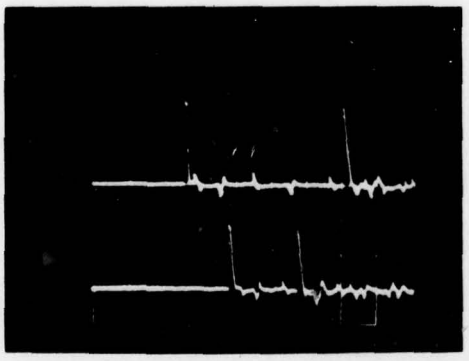

8b. upper trace: 100 m volt/div
lower trace: 500 m volt/div
horizontal: 1.0 msec/div
100 μ sec Heat Pulse
T_o = 1.63 °K

FIGURE 8 OSCILLOSCOPE TRACES SHOWING SECOND SOUND SHOCK WAVE REFLECTION FROM AN ENDWALL

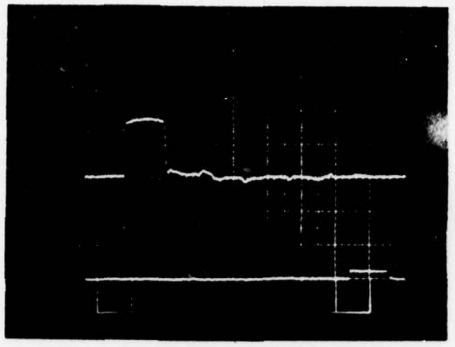

250 μ sec pulse duration
1.35 mK/div
200 μ sec/div

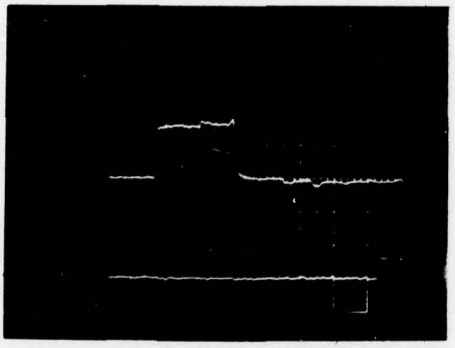

500 μ sec pulse duration
1.35 mK/div
200 μ sec/div

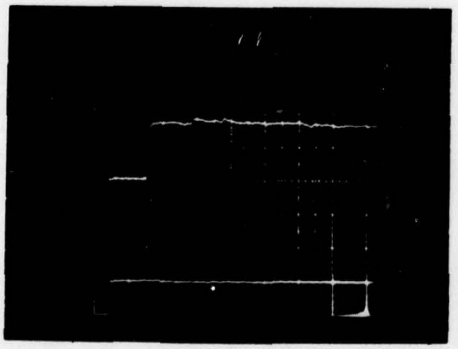

10 m sec pulse duration
1.35 mK/div
200 μ sec/div

FIGURE 9 OSCILLOSCOPE TRACES OF TYPICAL HEAT PULSES GENERATED BY VARIOUS DURATION VOLTAGE PULSES, T_o = 1.64°K

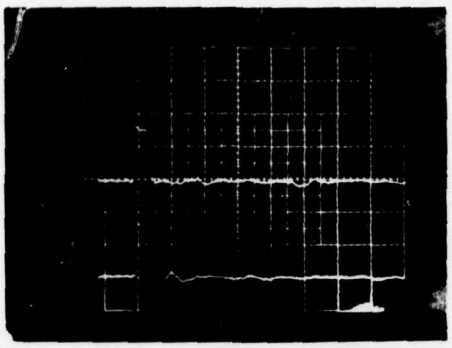

10a. 100 μ sec pulse

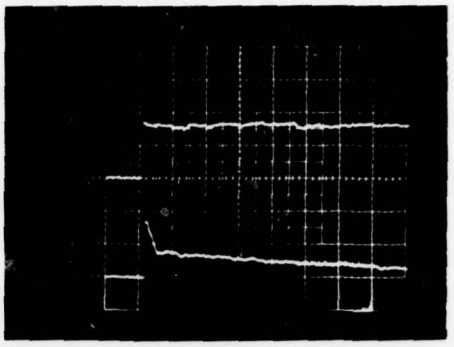

10b. 10 msec pulse

upper trace: 3.34 mK/div, sidewall detector
lower trace: 5.09 mK/div, center probe detector
horizontal: 200 μ sec/div

$T_o = 1.63\,^\circ K$

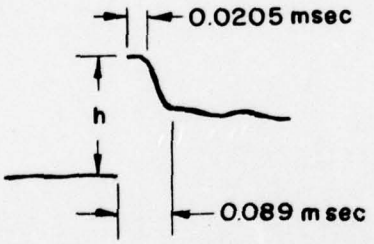

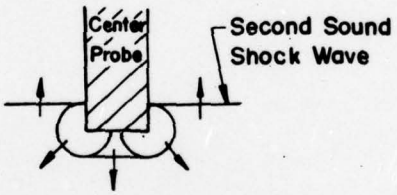

10 c.

FIGURE 10 SECOND SOUND SHOCK WAVES AS MEASURED BY SIDEWALL DETECTOR AND CENTER PROBE

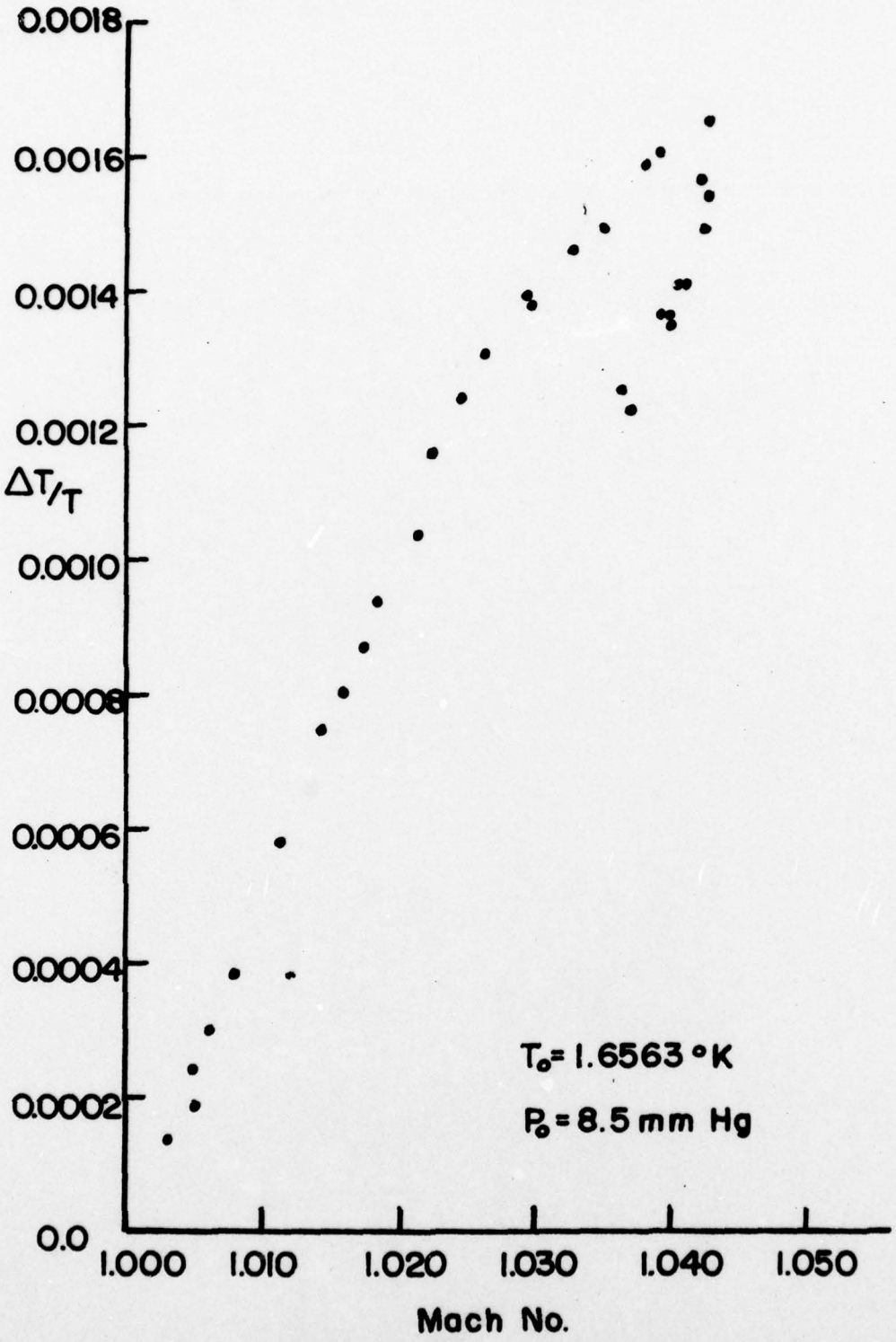

FIGURE 11 PLOT OF SHOCK STRENGTH VS. M, TANTALUM DETECTOR

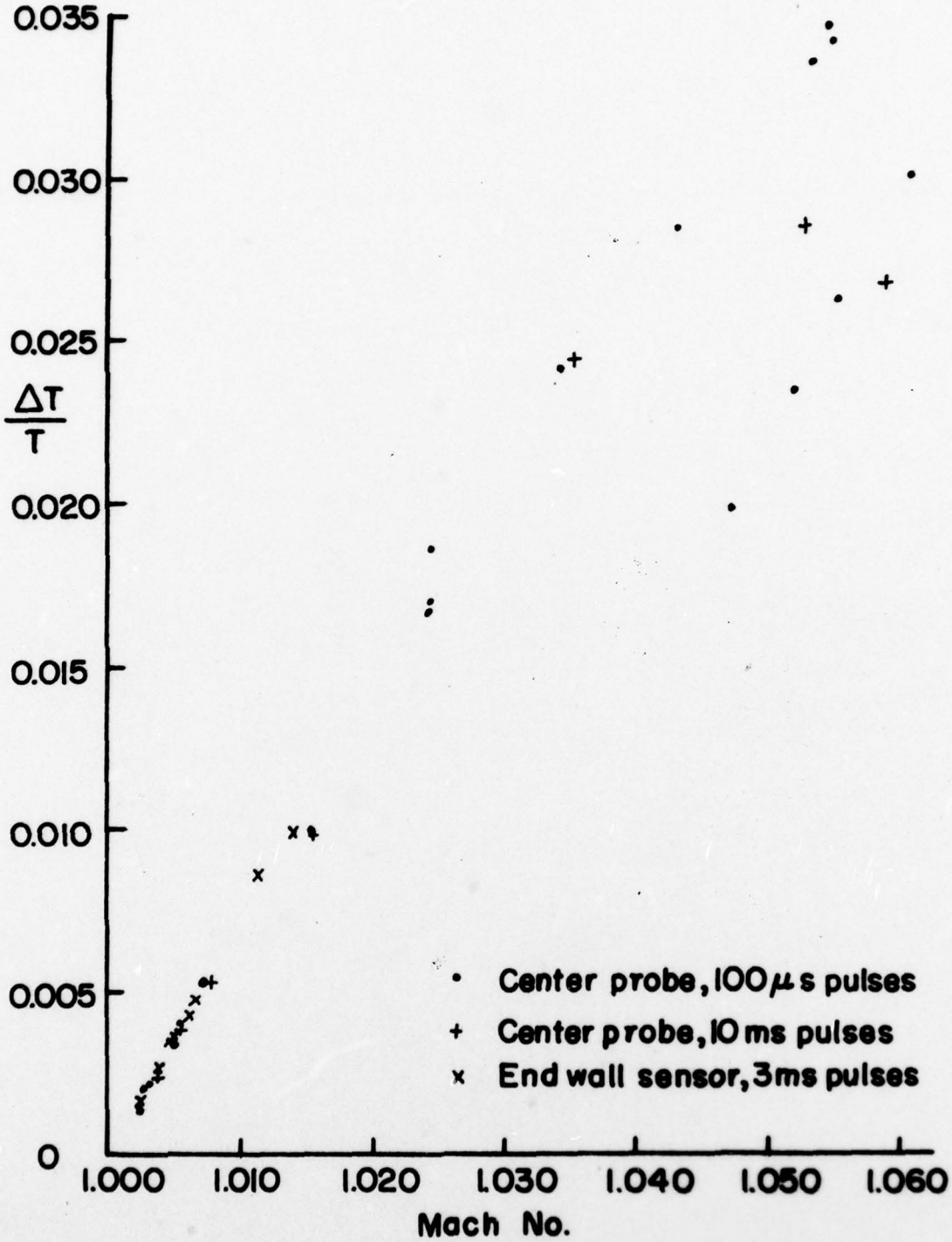

FIGURE 12 PLOT OF SHOCK STRENGTH VS. M, TIN ON GOLD ENDWALL DETECTOR AND CENTER PROBE

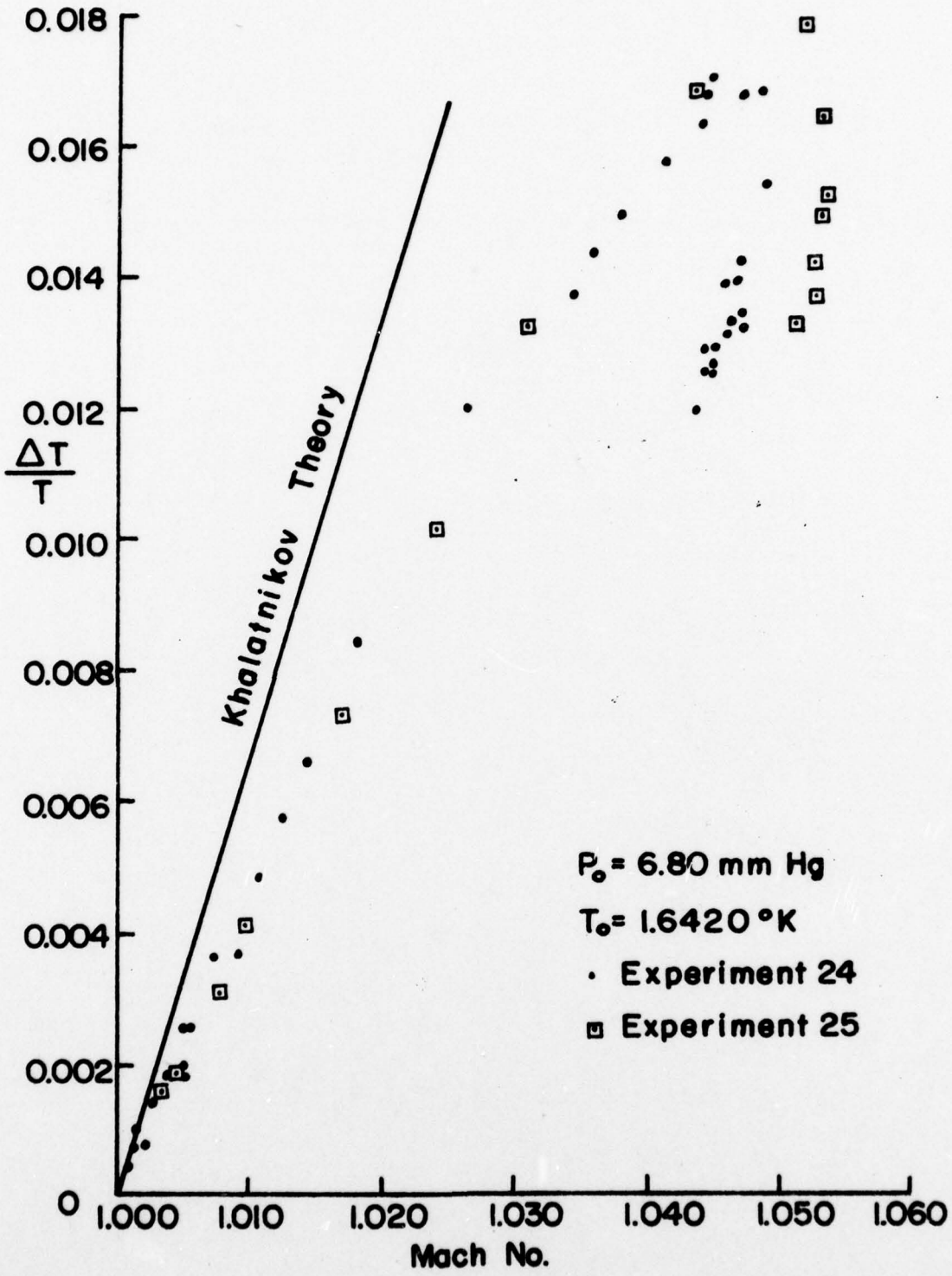

FIGURE 13 PLOT OF SHOCK STRENGTH VS M, TIN ON GOLD SIDEWALL DETECTORS

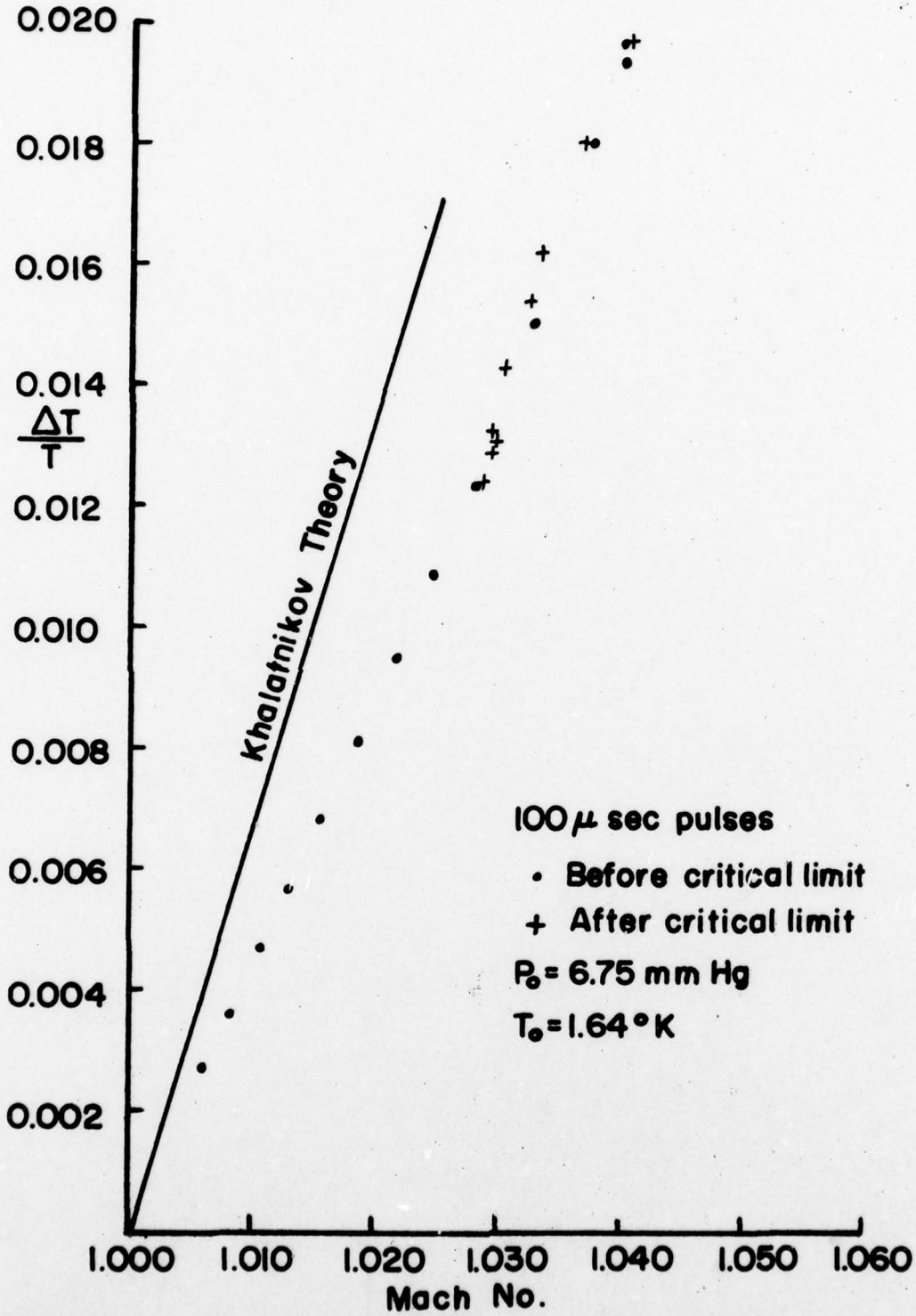

FIGURE 14 PLOT OF SHOCK STRENGTH VS. M, GOLD ON TIN DETECTOR TO DETECTOR

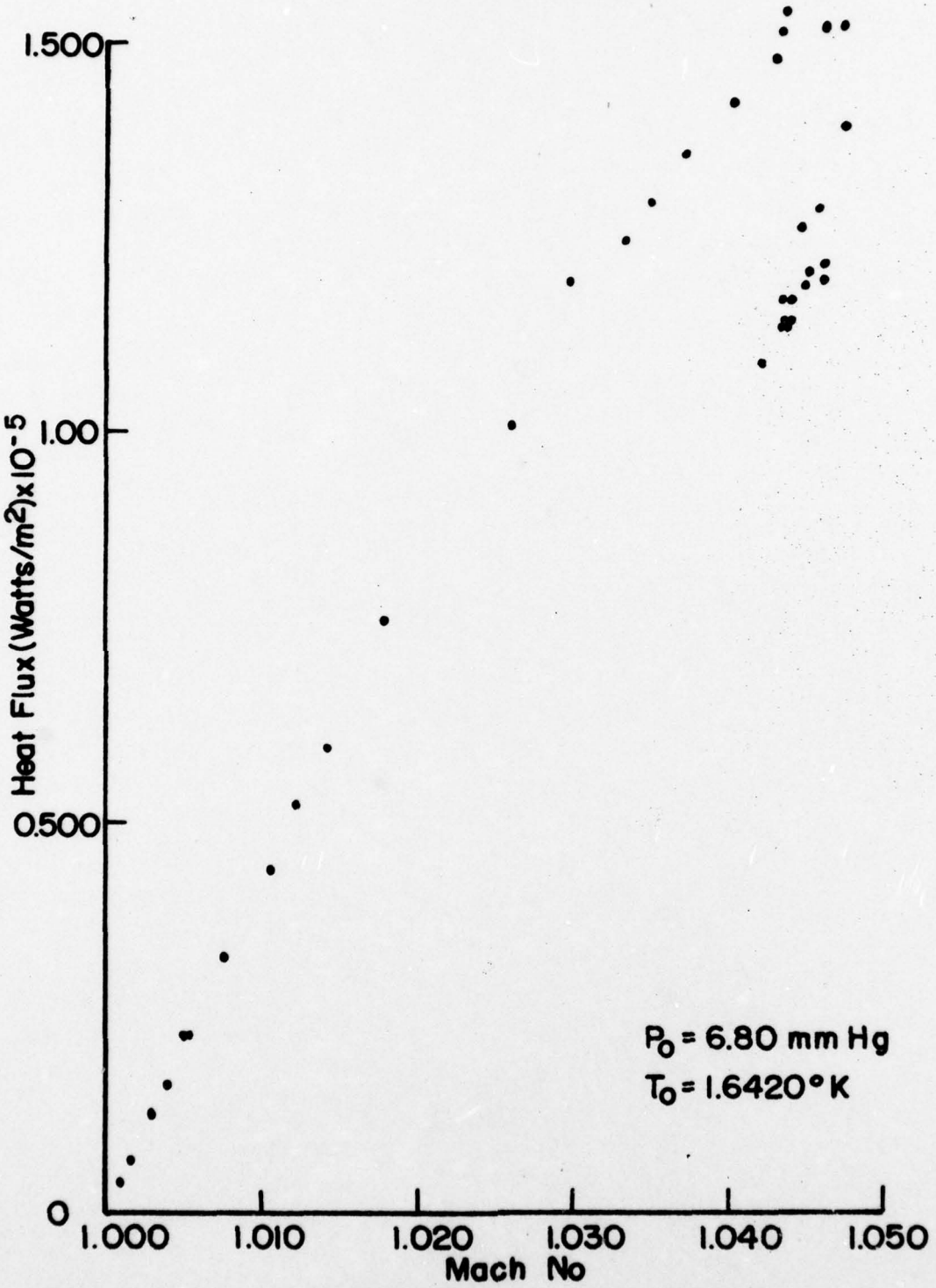

FIGURE 15 PLOT OF HEAT FLUX VS. M, EMITTER TO DETECTOR MEASUREMENTS

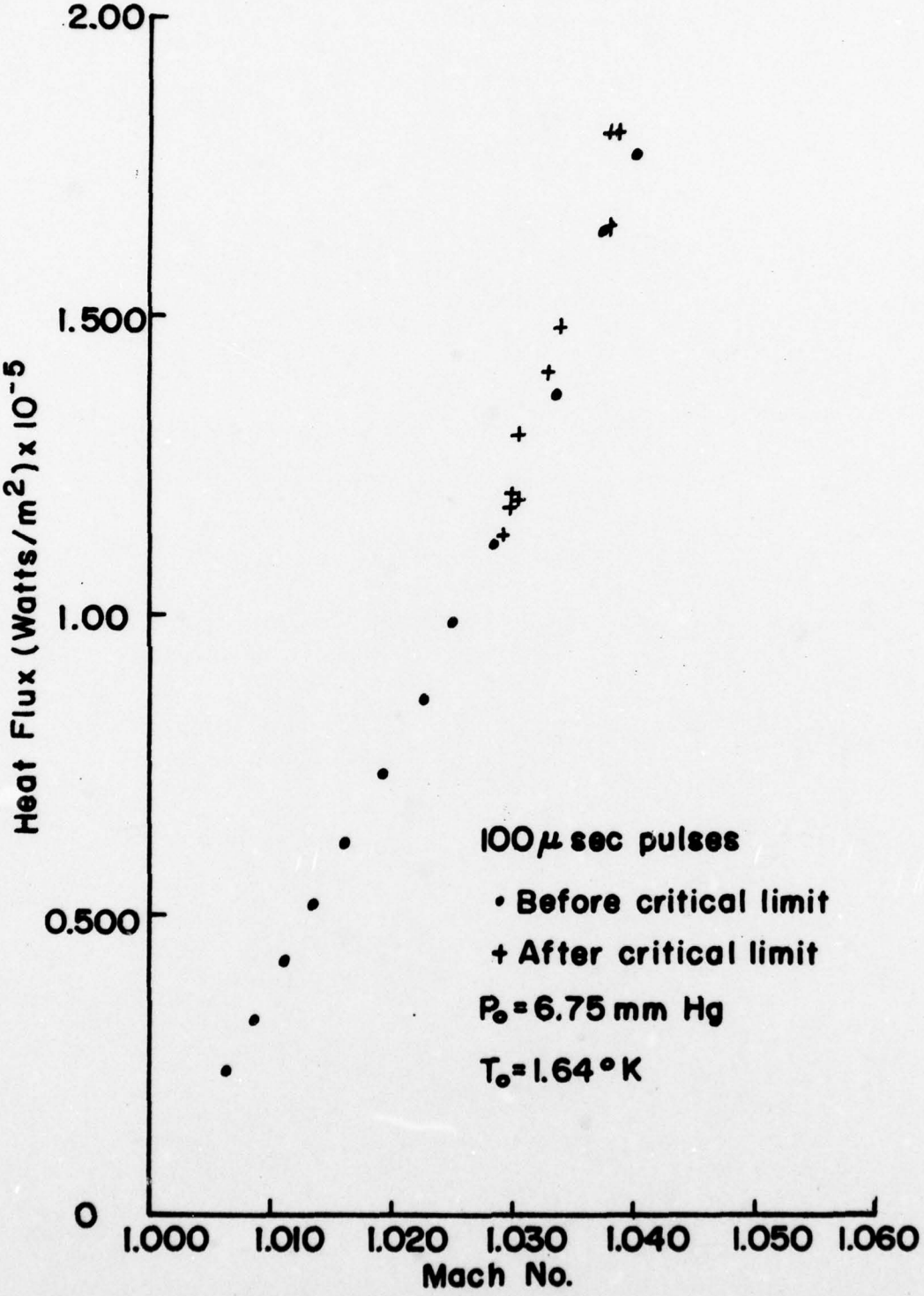

FIGURE 16 PLOT OF HEAT FLUX VS. M, DETECTOR TO DETECTOR MEASUREMENTS

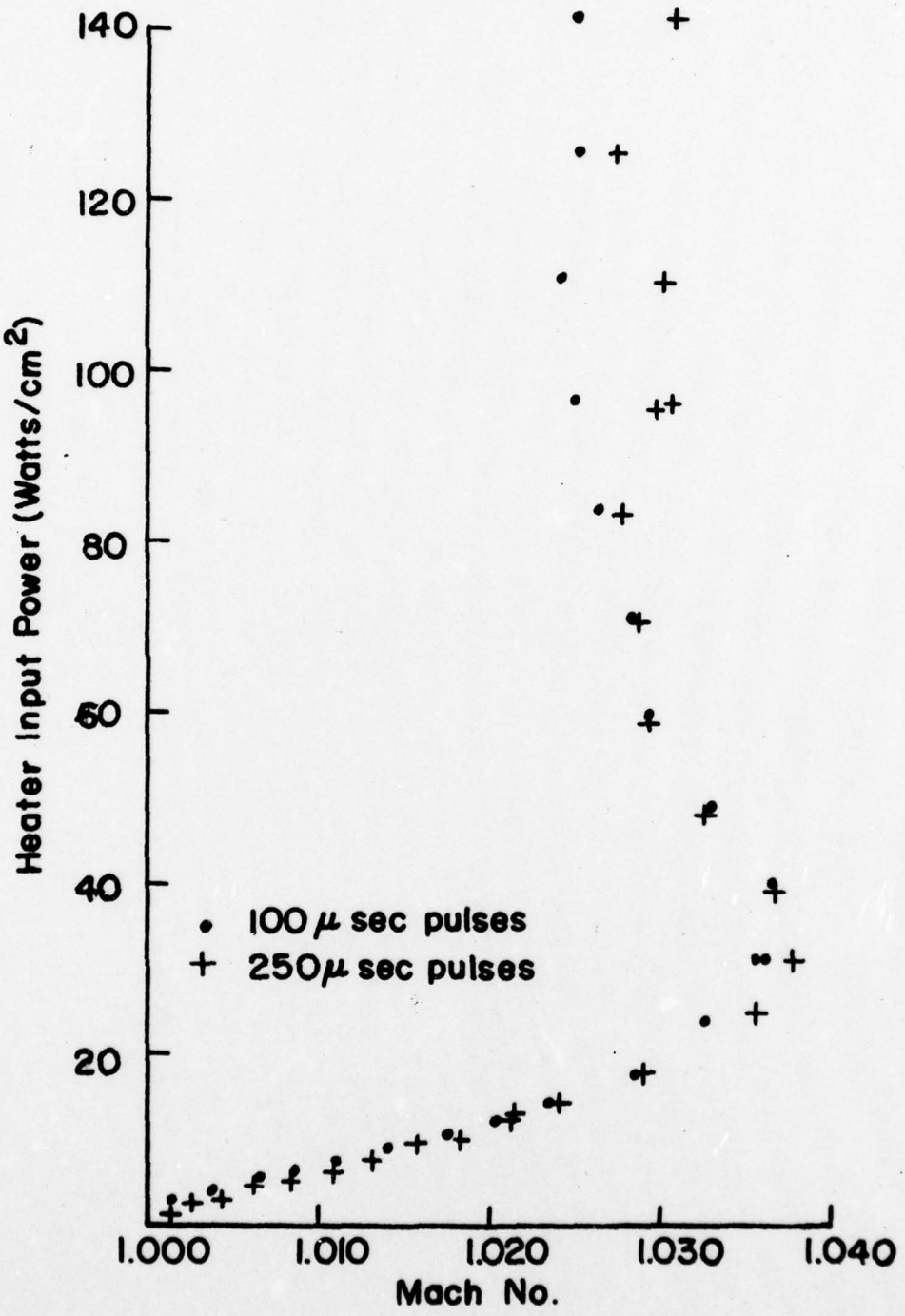

FIGURE 17 HEATER INPUT POWER VS. M, SIDEWALL DETECTOR

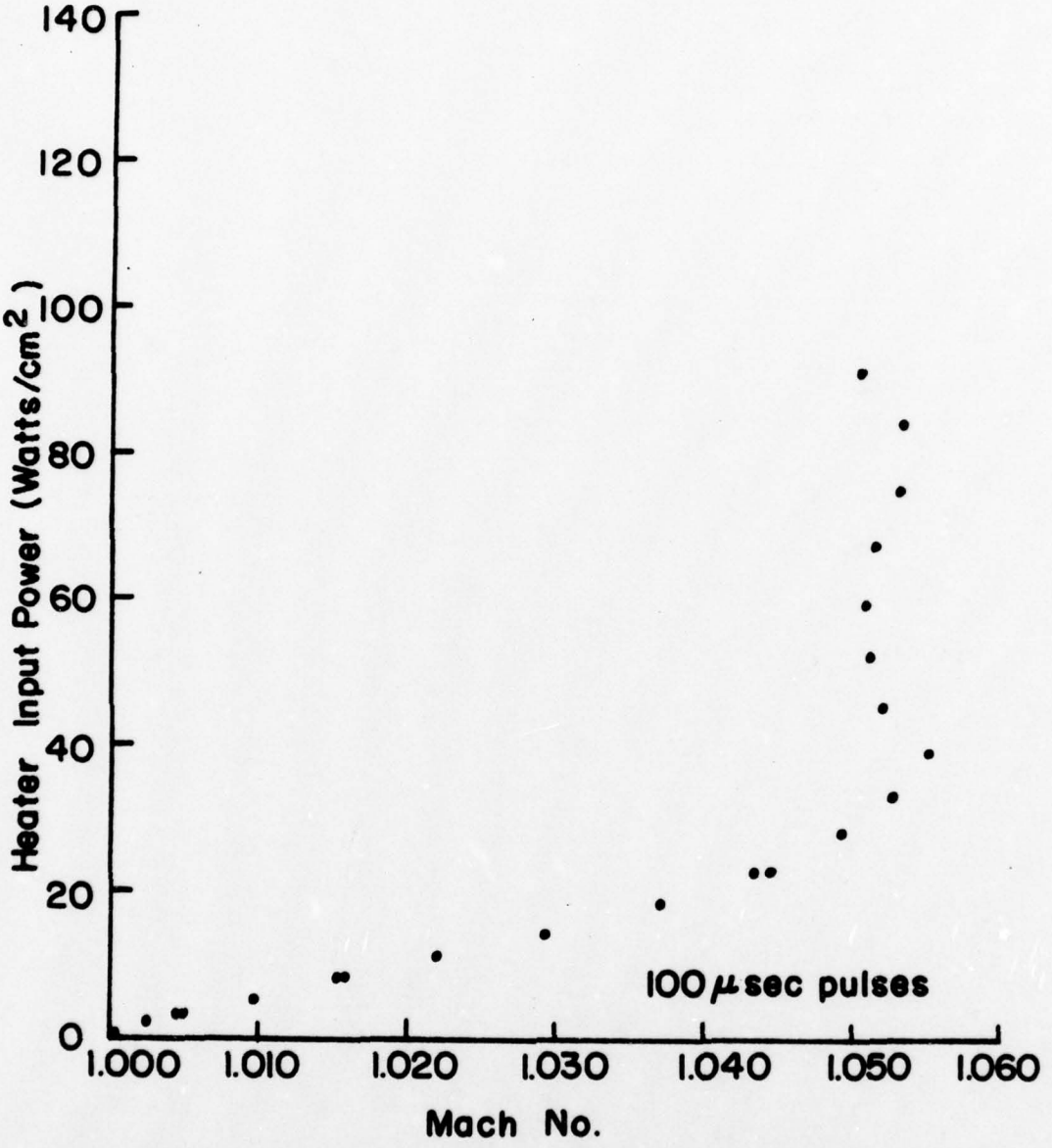

FIGURE 18 HEATER INPUT POWER VS. M, CENTER PROBE DETECTOR

SECTION D

Theoretical Calculation of Second-Sound Shock Wave Structure

Section D

LIST OF SYMBOLS

a_I	first sound speed
a_{II}	second sound speed
C	specific heat
p	pressure
s	specific entropy
T	temperature
U_s	shock velocity
v	bulk fluid velocity
v_n	normal fluid velocity
v_s	superfluid velocity
w	relative velocity
α	absorption coefficient of second sound
δ	shock thickness
η	normal viscosity
κ	thermal conductivity
ρ	mass density
θ	shock strength
μ	chemical potential
$\zeta_1, \zeta_2, \zeta_3$	second viscosities
ω	angular frequency
$( )_n$	normal fluid
$( )_s$	superfluid
$( )_0$	equilibrium state where $w = 0$
$( )_1$	equilibrium state where $w \neq 0$

Section D

LIST OF SYMBOLS (cont.)

$( )'$	perturbation from equilibrium state
$\Delta( )$	jump between equilibrium states
$\tilde{(\ )}$	thermodynamic function of w^2

I. INTRODUCTION

One of the most unusual and useful properties of liquid Helium II is its ability to propagate heat as a temperature wave. This method of transporting heat is totally analogous to the distribution of density perturbations in any fluid by pressure or "sound waves". And just as finite amplitude pressure waves will steepen into shock waves, finite amplitude temperature waves in He II will steepen into "second sound shock waves". The structure of these temperature shock waves is the subject of the following discussion.

Calculation of shock waves in a complex medium such as Helium II can be done using techniques from singular perturbation theory. The solution sought is one consisting of two equilibrium states which are connected by a thin shock layer or shock front. The jump conditions between the two equilibrium states form the outer solution, which is gotten by neglecting all the dissipative terms. These terms are zero in the outer solution since there are no gradients in any of the dependent variables in the equilibrium states. Gradients do exist and are important in the shock layer. In fact it is the balance between the dissipative terms and the nonlinear steepening terms which governs the shock structure.

The model of Helium II, which serves as a starting point for the following calculations, is the two fluid theory as set down by L. D. Landau.[1] The derivation begins by integrating the steady, one-dimensional equations for a superfluid and then evaluating the constants of integration using values for one of the equilibrium states. This results in the shock

equations presented in tables 3 and 4. Next the shock equations, in the linearized dissipationless approximation, are solved to obtain solutions for steady, first and second sound waves. These solutions shows that, to first order, the quantities characterizing a second sound wave are perturbations in the temperature, entropy, normal mass fraction, and relative velocity between the normal and superfluid motions; variations in pressure and density are of higher order. Because this is a linearized solution to a set of basically nonlinear equations, the results are valid only in the limit vanishing amplitude. Finite-amplitude waves, which steepen thru nonlinear processes into shock waves, have an amplitude-dependent velocity. The shock velocity can only be calculated if the nonlinear terms are retained. This is done for second sound shock waves by solving the dissipationless shock equations to second order in characterizing variables: T', s', ξ', w.

In the shock layer the gradients become very large so that even though the kinetic coefficients are small, their products are dominate terms in the equations. These dissipative terms are of order $(T')^2 \sim w^2$; that is they are second order in the characterizing variables for second sound. Therefore, to balance these terms, the shock equations must be solved with all the other second order terms being retained. The order of the dissipative terms depends on the fact that for weak shock waves, the shock thickness is inversely proportional to the shock strength, θ, which will be taken as the temperature jump normalized by an equilibrium state temperature. (This fact will be derived later when the method of stretching and matched asymptotic expansions is used to solve for the

shock structure.) The shock layer must therefore be scaled by $1/\theta$, which means the derivative with respect to the spatial dimension, x, must be order θ. Since the temperature and velocity perturbations are also of this order their derivatives must be order $\theta^2 \propto w^2$.

II. DERIVING THE SHOCK EQUATIONS

Calculation of shock wave jump conditions traditionally makes use of conservation equations for mass, momentum, and energy; these quantities are conserved from one equilibrium state to the other across the shock, even though the details within the shock itself may be unknown. The same approach is applicable to temperature shocks in He II, except in this case an additional equation describing the superfluid velocity field must be included.

The major problem in calculating the shock conditions in superfluid Helium arises because the thermodynamics of this liquid are not completely known. The thermodynamic variables of He II are functions of two ordinary variables, like pressure and temperature, plus an extra variable--the relative velocity between the normal and superfluid motions. Thus, the thermodynamics of He II are intrinsically connected with the velocity fields; that is, there is no way to separate the thermodynamics from the velocity field dependence, such as can be done with an ordinary one-component fluid. This leads to complicated equations, but does not represent a fundamental problem in the calculations. What is more significant, is that the dependence of the thermodynamic variables on the relative velocity is not known. The only recourse to date has been to expand the thermodynamics in terms of w, the relative velocity, which must be assumed small in some sense. This was done by Landau[1] and is reproduced in Table 1. It should be noted that the thermodynamics are expansions in the square of the relative velocities and that only the coefficients for the terms second order in w are known. This makes it

TABLE 1

Thermodynamic Functions Expanded in Terms of the Relative Velocity

$$\tilde{\mu}(p,T,w^2) = \mu(p,T) - \frac{1}{2}\frac{\rho_n}{\rho} w^2 + O(w^4)$$

$$\tilde{s}(p,T,w^2) = s(p,T) + \frac{1}{2}\xi_T w^2 + O(w^4)$$

$$\frac{1}{\rho(\tilde{p},T,w)} = \frac{1}{\rho(p,T)} - \frac{1}{2}\xi_p w^2 + O(w^4)$$

$$\tilde{\xi}(p,T,w^2) = \xi(p,T) + O(w^4)$$

$$\xi \equiv \frac{\rho_n}{\rho}$$

where $$\xi_p \equiv \left(\frac{\partial}{\partial p}\frac{\rho_n}{\rho}\right)_T$$

$$\xi_T \equiv \left(\frac{\partial}{\partial T}\frac{\rho_n}{\rho}\right)_p$$

NOTE: When the generalized thermodynamic variables, which are functions of pressure, temperature and relative velocity, are used in context with the variables that can be measured, which are functions of pressure and temperature only, then the former will be denoted by a tilda as shown above while the latter will be left unadorned.

TABLE 2

The Steady, One-Dimensional Form of the Two-Fluid Equations Including Dissipation

MASS: $$\frac{d}{dx} j = 0$$

MOMENTUM: $$\frac{d}{dx}\left[\tilde{\rho} v^2 + \frac{\tilde{\rho}_n \tilde{\rho}_s}{\tilde{\rho}} w^2 + p + \tau \right] = 0$$

SUPERFLUID: $$\frac{d}{dx}\left[\tilde{\mu} + \frac{1}{2} v_s^2 + h \right] = 0$$

ENERGY: $$\frac{d}{dx}\left[j(\tilde{\mu} + \frac{1}{2} v_s^2) + \tilde{\rho} s T v_n + \tilde{\rho}_n v_n^2 w + Q' \right] = 0$$

where: $$j \equiv \tilde{\rho} v \equiv \tilde{\rho}_n v_n + \tilde{\rho}_s v_s$$

$$w \equiv v_n - v_s$$

$$\tau = -(\frac{4}{3}\eta + \zeta_2) \frac{dv_n}{dx} + \zeta_1 \frac{d}{dx}(\tilde{\rho}_s w)$$

$$h = \zeta_3 \frac{d}{dx}(\tilde{\rho}_s w) - \zeta_1 \frac{dv_n}{dx}$$

$$Q' = -\kappa \frac{dT}{dx} - (\frac{4}{3}\eta + \zeta_2) v_n \frac{dv_n}{dx} + \zeta_1 \tilde{\rho}_s w \frac{dv_n}{dx}$$

$$+ \zeta_1 v_n \frac{d}{dx}(\tilde{\rho}_s w) - \zeta_3 \rho_s w \frac{d}{dx}(\tilde{\rho}_s w)$$

possible to solve the shock equations to third order in w, but no higher. Since w is a first order quantity in a second sound shock wave, this necessarily means that the results to be obtained are valid only for weak temperature shocks.

The following derivations are done in the reference frame which travels along with the shock wave--the shock-stationary frame. In this reference frame the shock profile is assumed steady. In the laboratory frame, where the undisturbed fluid is at rest, the shock will be traveling in the negative x-direction; that is, the shock velocity, U_S, will be negative. In the shock-stationary frame the mass flux, j, therefore will be in the positive x-direction.

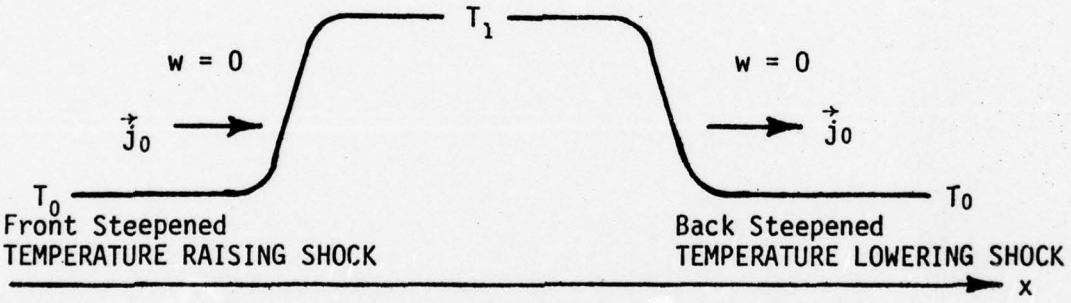

The shock profiles for two types of temperature shocks possible in He II are shown above. The front steepened one is a temperature raising shock in which the entropy density following the shock is greater than before it. The back steepened one is a temperature lowering shock; in this case the entropy density is decreased following passage of the shock front.

In the chosen reference frame the applicable equations describing a plane shock wave are the steady, one-dimensional form of the conservation

equations previously mentioned. This set of equations is reproduced as Table 2. The dissipative effects are included so that a shock profile and thickness can be calculated. The form of the dissipative terms follows from a consistent derivation made by Landau and Khalatnikov[2] which requires the assumption that the superfluid is free of vorticity; this is no restriction in the analysis which follows.

The one dimensional equations are easily integrated and the constants of integration are evaluated for the equilibrium state where the relative velocity is zero. This state will be indicated by a subscript zero. The other equilibrium state will be denoted by a subscript one. Unsubscripted variables will be considered as functions of x. For example, the integrated equation for mass conservation is:

$$(1) \qquad j \equiv \tilde{\rho} v = -\rho_0 U_s$$

This can be solved for the bulk velocity, v, to get:

$$(2) \qquad v = \frac{-\rho_0}{\tilde{\rho}} U_s = -\frac{\rho_0}{\rho} U_s + \tfrac{1}{2}\rho_0 U_s w^2 \xi_p + O(w^4)$$

where the last step was to expand the density in terms of w^2. The thermodynamic variables without the tilda are functions only of pressure and temperature. The other three equations can be integrated and expanded in terms of w^2; then the bulk velocity, v, can be eliminated by use of the previous formula. The resulting "shock equations" can be found in Table 3. Two equations which are linear combinations of the three original shock equations and which are useful when calculating second sound shock waves are presented in Table 4.

The same procedure of expanding in the relative velocity and then eliminating any bulk velocity dependence must also be applied to the dissipative terms, τ, h, and Q'. From the definition of v_n we have:

$$v_n \equiv v + \frac{\tilde{\rho}_s}{\tilde{\rho}} w = v + \frac{\rho_s}{\rho} w + O(w^4)$$

By using equation (2), the normal fluid velocity can be expanded in terms of w and the shock velocity with the result:

$$(3) \quad v_n = -\frac{\rho_0}{\rho} U_s + \frac{\rho_s}{\rho} w + \tfrac{1}{2}\rho_0 U_s w^2 \xi_p + O(w^4)$$

When calculating the derivatives, use will be made of the fact that the shock thickness is inversely proportional to the shock strength. For second sound shocks this means that the spatial dimension, x, is scaled by w^{-1}:

$$\frac{d}{dx} \sim w$$

With this simplification, the normal velocity gradient written out to third order in w is:

$$(4) \quad \frac{d}{dx} v_n = (\rho_s w - \rho_0 U_s) \frac{d}{dx} \frac{1}{\rho} + \frac{1}{\rho} \frac{d}{dx} \rho_s w + \tfrac{1}{2}\rho_0 U_s \frac{d}{dx} \xi_p w^2 + O(w^4)$$

The product of the normal velocity with equation (4) is:

$$(5) \quad v_n \frac{dv_n}{dx} = \frac{\rho_0}{\rho} U_s (\rho_0 U_s - 2 \rho_s w) \frac{d}{dx} \frac{1}{\rho} + \frac{1}{\rho^2} (\rho_s w - \rho_0 U_s) \frac{d}{dx} \rho_s w$$
$$- (\tfrac{1}{2}\rho_0 U_s^2) \frac{\rho_0}{\rho} \frac{d}{dx} \xi_p w^2 + O(w^4)$$

These results allow for further expansion and simplification of the kinectic fluxes which are valid for second sound shocks. These expansions are reproduced in Table 5.

TABLE 3

Shock Equations

MOMENTUM

$$\frac{p-p_0}{\rho U_s^2} = \left(1 - \frac{\rho_0}{\rho}\right)\frac{\rho_0}{\rho} - \left[\frac{\rho_n\rho_s}{\rho^2} - \frac{\rho_0}{\rho}\left(\tfrac{1}{2}\rho_0 U_s^2\,\xi_p\right)\right]\left(\frac{w}{U_s}\right)^2 - \frac{\tau}{\rho U_s^2} + O(w^4)$$

SUPERFLUID

$$\frac{\mu-\mu_0}{U_s^2} = \tfrac{1}{2}\left[1 - \left(\frac{\rho_0}{\rho}\right)^2\right] - \frac{\rho_n}{\rho}\frac{\rho_0}{\rho}\left(\frac{w}{U_s}\right) + \tfrac{1}{2}\left[\frac{\rho_n\rho_s}{\rho^2} + \frac{\rho_0}{\rho}\left(\rho_0 U_s\,\xi_p\right)\right]\left(\frac{w}{U_s}\right)^2$$
$$+ \frac{\rho_n}{\rho}\left(\rho_0 U_s^2\xi_p\right)\left(\frac{w}{U_s}\right)^3 - \frac{h}{U_s^2} + O(w^4)$$

TOTAL ENERGY

$$\frac{sT - s_0T_0}{U_s^2} = \left[\left(\frac{\rho_0}{\rho}\right)^2 + \frac{\rho_s}{\rho_n}\frac{sT}{U_s^2}\right]\frac{\rho_n}{\rho_0}\left(\frac{w}{U_s}\right) - \left[2\frac{\rho_s}{\rho} + \tfrac{1}{2}\left(\frac{\rho}{\rho_n}T\xi_T\right)\right]\frac{\rho_n}{\rho}\left(\frac{w}{U_s}\right)^2$$
$$+ \left[\left(\frac{\rho_s}{\rho}\right)^2 + \tfrac{1}{2}\frac{\rho_s}{\rho}\left(\frac{\rho}{\rho_n}\xi_T T\right) - \frac{\rho_0}{\rho}\left(\rho_0 U_s^2\right)\xi_p\right]\frac{\rho_n}{\rho_0}\left(\frac{w}{U_s}\right)^3$$
$$+ \frac{Q'}{\rho_0 U_s^3} + \frac{h}{U_s^2} + O(w^4)$$

NOTE: Since these equations make use of the expanded thermodynamic functions, they are strictly valid only when the relative velocity is small.

TABLE 4

Shock Equations Useful for Second Sound Shock Waves

"W" EQUATION

$$\left(\frac{\mu-\mu_0}{U_s^2}\right)-\left(\frac{p-p_0}{\rho U_s^2}\right)=\tfrac{1}{2}\left(1-\frac{\rho_0}{\rho}\right)^2-\frac{\rho_n}{\rho}\cdot\frac{\rho_0}{\rho}\left(\frac{w}{U_s}\right)+\frac{3}{2}\frac{\rho_n\rho_s}{\rho^2}\left(\frac{w}{U_s}\right)^2$$

$$+\frac{\rho_n}{\rho}\left(\rho_0 U_s^2\,\xi_p\right)\left(\frac{w}{U_s}\right)^3+\frac{\tau}{\rho U_s^2}-\frac{h}{U_s^2}+O(w^4)$$

MODIFIED ENERGY EQUATION

$$\frac{(\mu-\mu_0)}{U_s^2}+\frac{sT-S_0T_0}{U_s^2}-\frac{p-p_0}{\rho U_s^2}=\tfrac{1}{2}\left(1-\frac{\rho_0}{\rho}\right)^2+\frac{\rho_s}{\rho_0}\frac{sT}{U_s^2}\left(\frac{w}{U_s}\right)$$

$$-\tfrac{1}{2}\left[\frac{\rho_s}{\rho}+\left(\frac{\rho}{\rho_n}\,T\,\xi_T\right)\right]\frac{\rho_n}{\rho}\left(\frac{w}{U_s}\right)^2$$

$$+\left[\frac{\rho_s}{\rho}+\tfrac{1}{2}\left(\frac{\rho}{\rho_n}\,\xi_T T\right)\right]\left(\frac{\rho_s}{\rho}\right)\left(\frac{\rho_n}{\rho_0}\right)\left(\frac{w}{U_s}\right)^3$$

$$+\frac{Q'}{\rho_0 U_s^3}+\frac{\tau}{\rho U_s^2}+O(w^4)$$

AD-A065 301 CALIFORNIA INST OF TECH PASADENA GRADUATE AERONAUTIC--ETC F/G 20/13
NONLINEAR INTERACTIONS IN SUPERFLUID DYNAMICS: SUPERCRITICAL CO--ETC(U)
NOV 78 H W LIEPMANN, P L ROGERS, T N TURNER F44620-75-C-0038
UNCLASSIFIED AFOSR-TR-79-0130 NL

2 OF 2
AD
A065301

END
DATE
FILMED
4 -79
DDC

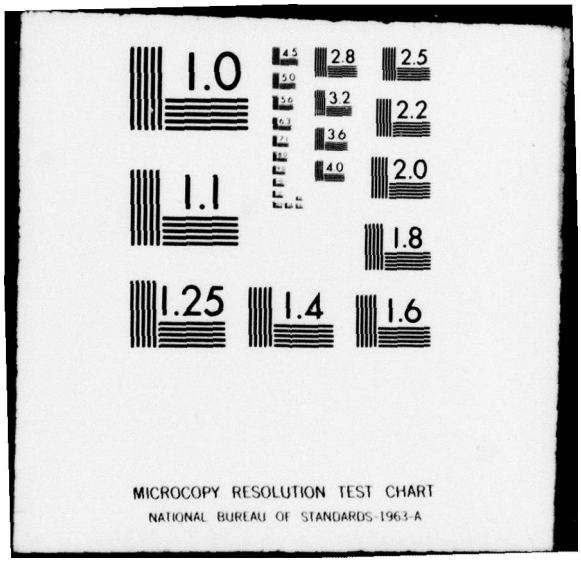
1.0
1.1
1.25
1.4
1.6
1.8
2.0
2.2
2.5
2.8
3.2
3.6
4.0
4.5
5.0
5.6
MICROCOPY RESOLUTION TEST CHART
NATIONAL BUREAU OF STANDARDS-1963-A

TABLE 5

Dissipative Terms for Second Sound Shocks

$$\tau = -\left(\frac{4}{3}\eta + \zeta_2\right)\left(\rho_s w - \rho_0 U_s\right)\frac{d}{dx}\frac{1}{\rho}$$
$$-\left(\frac{4}{3}\eta + \zeta_2 - \rho\zeta_1\right)\frac{1}{\rho}\frac{d}{dx}\rho_s w$$
$$-\tfrac{1}{2}\left(\frac{4}{3}\eta + \zeta_2\right)\rho_0 U_s \frac{d}{dx}\xi_p w^2 + O(w^4)$$

$$h = -\zeta_1\left(\rho_s w - \rho_0 U_s\right)\frac{d}{dx}\frac{1}{\rho}$$
$$-\left(\zeta_1 - \rho\zeta_3\right)\frac{1}{\rho}\frac{d}{dx}\rho_s w$$
$$-\tfrac{1}{2}\zeta_1 \rho_0 U_s \frac{d}{dx}\xi_p w^2 + O(w^4)$$

$$Q' = -\kappa\frac{dT}{dx} - \left(\frac{4}{3}\eta + \zeta_2\right)\frac{\rho_0}{\rho}\left(\rho_0 U_s^2\right)\frac{d}{dx}\frac{1}{\rho}$$
$$+ 2\left(\frac{4}{3}\eta + \zeta_2 - \tfrac{1}{2}\rho\zeta_1\right)\frac{\rho_0}{\rho}\left(\rho_s w\, U_s\right)\frac{d}{dx}\frac{1}{\rho}$$
$$+ \left(\frac{4}{3}\eta + \zeta_2 - \rho\zeta_1\right)\frac{\rho_0 U_s}{\rho^2}\frac{d}{dx}\rho_s w$$
$$- \left(\frac{4}{3}\eta + \zeta_2 - 2\rho\zeta_1 + \rho^2\zeta_3\right)\frac{\rho_s w}{\rho^2}\frac{d}{dx}\rho_s w$$
$$+ \left(\frac{4}{3}\eta + \zeta_2\right)\frac{\rho_0}{\rho}\left(\tfrac{1}{2}\rho_0 U_s^2\right)\frac{d}{dx}\xi_p w^2 + O(w^4)$$

NOTE: These equations, besides being expansions in the relative velocity, make use of the fact that d/dx is of order w. Thus these equations are strictly valid only for weak second sound shock waves.

III. LINEARIZED SOLUTION

Now since the shock waves under consideration are assumed small, the thermodynamic functions may be expanded further in terms of pressure and temperature perturbations, p' and T', defined by:

$$p \equiv p_0 + p'$$

$$T \equiv T_0 + T'$$

For liquid He II the coefficient of thermal expansion is very small. Therefore it will be neglected in the calculations to follow. Note that the assumption that the coefficient of thermal expansion is zero is equivalent to assumming that the entropy is a function only of temperature and that density is a function only of pressure. Also the specific heat at constant pressure and volume are equivalent and will be denoted by C. Table 6 lists a set of thermodynamic perturbations expansions when this assumption is envoked.

In order to see the role the various thermodynamic variables play in the two forms of wave motion occurring in He II, a solution to the linearized equations will be sought first. To do this the shock equations of Table 4 will be expanded in terms of the pressure and temperature perturbations with only linear terms being retained. Now to solve for the jump conditions, the perturbations p', and T', and w, will become the differences between the two equilibrium states:

$$p' \to p_1 - p_0 \equiv \Delta p$$

$$T' \to T_1 - T_0 \equiv \Delta T$$

$$w \to w_1 \qquad \equiv \Delta w$$

TABLE 6

Thermodynamic Perturbation Expansions

Independent variables:

$$p = p_0 + p' \qquad T = T_0 + T'$$

where $\frac{p'}{p_0} << 1$ and $\frac{T'}{T_0} << 1$

Expansions of dependent variables:

$$\mu(p,T) = \mu_0 - s_0 T' + \frac{1}{\rho_0} p' - \left(\frac{C}{T}\right)_0 \frac{(T')^2}{2} - \left(\frac{1}{\rho^2 a_I^2}\right)_0 \frac{(p')^2}{2} + \ldots$$

$$s(T) = s_0 + \left(\frac{C}{T}\right)_0 T' + \left[\frac{1}{T}\left(\frac{dC}{dT}\right) + \frac{C}{T^2}\right]_0 \frac{(T')^2}{2} + \ldots$$

$$\rho(p) = \rho_0 + \frac{p'}{a_{I0}^2} + \left(\frac{d^2\rho}{dp^2}\right)_0 \frac{(p')^2}{2} + \ldots$$

$$sT - s_0 T_0 = (s + C)_0 T' + \left[\left(\frac{dC}{dT}\right) + \frac{C}{T}\right]_0 \frac{(T')^2}{2} + \ldots$$

$$\left(1 - \frac{\rho_0}{\rho}\right) = \frac{p'}{\rho_0 a_{I0}^2} + \ldots$$

$$\frac{\rho_n}{\rho} = \left(\frac{\rho_n}{\rho}\right)_0 + \xi_T T' + \xi_p p' + \ldots$$

$$\frac{\rho_s}{\rho} = \left(\frac{\rho_s}{\rho}\right)_0 - \xi_T T' - \xi_p p' + \ldots$$

where $C \equiv T\left(\frac{ds}{dT}\right)$ = specific heat

$a_I \equiv \sqrt{\left(\frac{\partial p}{\partial \rho}\right)_s}$ = speed of first sound

$$\xi_T \equiv \frac{\partial}{\partial T}\frac{\rho_n}{\rho} \qquad \xi_p \equiv \frac{\partial}{\partial p}\frac{\rho_n}{\rho}$$

NOTE: The coefficient of thermal expansion is assumed to be negligible, which implies that entropy is a function only of temperature and density is a function only of pressure. Also under this assumption, the specific heat ratio is equal to unity.

When this is done, all the dissipative terms will disappear because they depend only on derivatives, which are zero in the equilibrium states. Carrying out this procedure on the momentum, superfluid and total energy shock equations, yields the following set:

$$(6) \qquad \left(1 - \frac{U_s^2}{a_{I0}^2}\right) \Delta p = 0$$

$$(7) \qquad \frac{1}{\rho_0}\left(1 - \frac{U_s^2}{a_{I0}^2}\right) \Delta p - s_0 \Delta T + \frac{\rho_{n0}}{\rho_0} U_s \Delta w = 0$$

$$(8) \qquad (s_0 + C_0)\, \Delta T - \left[\frac{\rho_{s0}}{\rho_{n0}} s_0 T_0 + U_s^2\right] \frac{\rho_{n0}}{\rho_0} \frac{\Delta w}{U_s} = 0$$

For a nontrivial solution to exist the determinate of the coefficients of Δp, ΔT, and Δw must vanish. This requirement yields the following characteristic equation:

$$(9) \qquad \left(1 - \frac{U_s^2}{a_{I0}^2}\right)\left(\frac{\rho_{s0}}{\rho_{n0}} \frac{s_0^2 T_0}{C_0} - U_s^2\right) = 0$$

therefore:

$$U_s = \pm a_{I0}$$

$$\text{or} \quad U_s = \pm a_{II0}$$

where the second sound speed has been defined as:

$$(10) \qquad a_{II} = \sqrt{\frac{\rho_s}{\rho_n} \frac{s^2 T}{C}}$$

The result of this linearized analysis is simply to find steady first and second sound waves. Since a coordinate system in which the wave was assumed steady has been used throughout, only steady sound or

shock waves can be found. This first result is not a shock wave since there is no nonlinear steepening involved.

Using the second sound speed result in equation (8) yields the following relation:

$$(11) \qquad \Delta T = \left(\frac{\rho_n}{\rho_s}\right)_0 U_s \, \Delta w \ , \text{ for } U_s = a_{II0}$$

which can also be written as:

$$(12) \qquad \frac{\Delta w}{U_s} = \left(\frac{\rho}{\rho_s} \frac{C}{s}\right)_0 \theta \ , \text{ for } U_s = a_{II0}$$

where $\theta \equiv \frac{\Delta T}{T_0}$

Substituting this result into equation (7) reveals that the pressure jump, Δp, is zero to this level of approximation. Thus the pressure jump in a second sound wave must be of order w^2 or higher.* The only first order quantities in second sound waves will therefore be fluctuations of entropy, temperature, relative velocity, and normal fluid fraction (ρ_n/ρ).

---

* This statement must be modified when the coefficient of thermal expansion cannot be neglected. In that case the pressure jump will be of order w times the coefficient of thermal expansion which is still small, although not negligible.

IV. SOLVING FOR THE JUMP CONDITIONS AND SHOCK VELOCITY

When solving the shock equations to order w^2 for second sound it is useful to use the equations of Table 4, since terms involving pressure and density are order w^3. These equations expanded in terms of T' and w are:

$$(13)\quad \left(\frac{\rho_n}{\rho}\right)_0 U_s w - s_0 T' = \frac{3}{2}\left(\frac{\rho_n \rho_s}{\rho^2}\right)_0 w^2 - \xi_T T' U_s w + \left(\frac{C}{T}\right)_0 \frac{(T')^2}{2} + \frac{\tau}{\rho} - h + O(w^3)$$

$$(14)\quad C_0 T' - \left(\frac{\rho_s}{\rho} sT\right)_0 \frac{w}{U_s} = -\frac{1}{2}\left(\frac{\partial C}{\partial T}\right)_0 (T')^2 + \left[\frac{\rho_s}{\rho}(s+C) - ST\xi_T\right]_0 T' \frac{w}{U_s} - \frac{1}{2}\left[\frac{\rho_s}{\rho} + \left(\frac{\rho}{\rho_n} T\xi_T\right)\right]_0 \left(\frac{\rho_n}{\rho}\right)_0 w^2 + \frac{Q'}{\rho_0 U_s} + \frac{\tau}{\rho} + O(w^3) .$$

The dissipative terms similarily expanded but restricted to second sound shocks are:

$$(15)\quad \frac{\tau}{\rho} - h = -\left(\frac{4}{3}\frac{\eta}{\rho} + \frac{\zeta_2}{\rho} - 2\zeta_1 + \rho\zeta_3\right)_0 \left(\frac{\rho_s}{\rho}\right)_0 \frac{dw}{dx} + O(w^3)$$

$$(16)\quad \frac{Q'}{\rho_0 U_s} + \frac{\tau}{\rho} = -\frac{\kappa}{\rho_0 U_s}\frac{dT}{dx} + O(w^3)$$

From the first order solutions for second sound (see Eq. 12):

$$w = \frac{\rho_0 s_0}{\rho_{n0} U_s} T' + O(T')^2$$

This expression may be substituted into the second order terms of equations (13) thru (16) to eliminate w, since the error involved will be of third order. This substitution may not be made into the first order terms however, so there will still be a linear dependence of w in the two shock equations. The result of this simplification is the following set

of four equations:

$$(17)\quad \left(\frac{\rho_n}{\rho}\right)_0 U_s w - s_0 T' = \left(\frac{s}{T}\right)_0 \left[2\frac{C}{s} - \left(\frac{\rho}{\rho_n} T\xi_T\right)\right]_0 (T')^2 + \frac{\tau}{\rho} - h$$

$$(18)\quad C_0 T' - \left(\frac{\rho_s}{\rho} sT\right)_0 \frac{w}{U_s} = \frac{C_0}{T_0}\frac{a_{II0}^2}{U_s^2}\left[\frac{1}{2} + \frac{C}{s} - \frac{1}{2}\left(\frac{T}{C}\frac{\partial C}{\partial T}\right) - \left(\frac{3}{2}\frac{\rho_n}{\rho_s} + \frac{1}{2}\right)\left(\frac{\rho}{\rho_n} T\xi_T\right)\right]_0 (T')^2 + \frac{Q'}{\rho_0 U_s} + \frac{\tau}{\rho}$$

$$(19)\quad \frac{\tau}{\rho} - h = -\left(\frac{4}{3}\frac{\eta}{\rho} + \frac{\zeta_2}{\rho} - 2\zeta_1 + \rho\zeta_3\right)_0 \left(\frac{\rho_s s}{\rho_n U_s}\right)_0 \frac{dT}{dx}$$

$$(20)\quad \frac{Q'}{\rho_0 U_s} + \frac{\tau}{\rho} = -\frac{k}{\rho_0 U_s}\frac{dT}{dx}$$

Finally w can be eliminated by multiplying thru equation (17) by $(T/s)_0$ and equation (18) by $(T/C)_0\ (U_s/a_{II_0})^2$, and adding. The result is:

$$(21)\quad \left(\frac{U_s^2}{a_{II_0}^2} - 1\right) T_0 T' = \left[\frac{1}{2} + 3\frac{C}{s} - \frac{1}{2}\left(\frac{T}{C}\frac{\partial C}{\partial T}\right) - \frac{3}{2}\left(\frac{\rho_n}{\rho_s} + 1\right)\left(\frac{\rho}{\rho_n} T\xi_T\right)\right]_0 (T')^2 + \left(\frac{T}{C}\right)_0 \left[\frac{Q'}{\rho_0 U_s} + \frac{\tau}{\rho} + \left(\frac{\tau}{\rho} - h\right)\left(\frac{C}{s}\right)_0\right]$$

Note when writing down the dissipative terms use was made of the fact that these terms are of order w^2 and that U_s^2 equals $a_{II_0}^2$ plus a correction of order w.

From this point the jump equations can be simply solved by letting $T' \to \Delta T$ and by noting that the dissipative terms disappear because two equilibrium states are being used.

$$(22)\quad \left(\frac{U_s^2}{a_{II_0}^2} - 1\right) = \left[\frac{1}{2} + 3\frac{C}{s} - \frac{1}{2}\left(\frac{T}{C}\frac{\partial C}{\partial T}\right) - \frac{3}{2}\left(\frac{\rho_n}{\rho_s} + 1\right)\left(\frac{\rho}{\rho_n} T\xi_T\right)\right]_0 \frac{\Delta T}{T_0}$$

$$= \left[T\frac{\partial}{\partial T}\log\left(a_{II}^3 \frac{C}{T}\right)\right]_0 \theta$$

This yields Khalatnikov's well known second sound shock velocity formula[3]:

$$(23)\quad U_s = \pm a_{II_0}\left(1 + \frac{1}{2} b_0\theta\right)$$

where b(p,T) is a thermodynamic function defined by:

$$(24)\quad b(p,T) \equiv T\frac{\partial}{\partial T}\log\left(a_{II}^3 \frac{C}{T}\right)$$

This solution to shock velocity can be substituted into equation (17) to yield a second order result for the relative velocity jump. Equation (17) rewritten as a jump equation and solving for Δw is:

$$(25)\quad \frac{\Delta w}{a_{II_0}} = \left(\frac{\rho s}{\rho_n T}\right)_0 \frac{T_0 \Delta T}{U_s a_{II_0}}\left[1 + \left(2\frac{C}{s} - \frac{\rho}{\rho_n} T\xi_T\right)_0 \theta\right]$$

but from equation (22):

$$\frac{1}{U_s} = -\frac{1}{a_{II_0}}\left[1 - \frac{b_0}{2}\theta\right]$$

which substituted into equation (25) yields:

$$(26)\quad \frac{\Delta w}{a_{II_0}} = -\left(\frac{\rho}{\rho_s}\frac{C}{s}\right)_0 \theta\left\{1 + \frac{1}{4}\left[2\frac{C}{s} + \left(\frac{T}{C}\frac{\partial C}{\partial T}\right) + \left(3\frac{\rho_n}{\rho_s} - 1\right)\left(\frac{\rho}{\rho_n} T\xi_T\right) - 1\right]_0 \theta\right\}$$

$$= -\left(\frac{\rho}{\rho_s}\frac{C}{s}\right)_0 \theta\left\{1 + \frac{1}{2} T\frac{\partial}{\partial T}\left[\log a_{II}\frac{C}{T}\left(\frac{\rho}{\rho_s}\right)^2\right]\theta\right\}$$

V. SHOCK STRUCTURE SOLUTION

The shock structure can now be solved directly from equation (21) which is rewritten below:

$$(27)\qquad \left[\frac{U_s^2}{a_{II_0}^2} - 1\right] T_0 T' = b_0 (T')^2 + \frac{T_0}{\rho_0 a_{II_0}} \left[\frac{\kappa}{C} + \frac{\rho_s}{\rho_n}\left(\frac{4}{3}\eta + \zeta_2 - 2\rho\zeta_1 + \rho^2\zeta_3\right)\right]_0 \frac{dT}{dx}$$

This equation can be rearranged with the aid of the shock velocity result to the following nondimensional form:

$$(28)\qquad \frac{d\overline{T}}{dy} = \theta\overline{T} - \overline{T}^2$$

where $$\overline{T} \equiv \frac{T - T_0}{T_0}$$

$$y \equiv \frac{b_0}{a_{II_0}^2 A_0}\, x$$

$$(29)\qquad A(p,T) \equiv \frac{1}{\rho a_{II}^3}\left[\frac{\kappa}{C} + \frac{\rho_s}{\rho_n}\left(\frac{4}{3}\eta + \zeta_2 - 2\rho\zeta_1 + \rho^2\zeta_3\right)\right]$$

Equation (28) and the entire analysis which preceded, are valid only for weak shock waves; that is, the shock strength, θ, must be much smaller than unity.

The remaining question that needs to be answered before solving equation (28) concerns whether quadratic or just linear terms are required to balance the differential term. The shock layer is a very narrow part of the entire shock solution when expressed in the nondimensional variable y; therefore it is useful to rewrite the equation in stretched

coordinates as follows:

$$\text{Set} \quad \bar{y} \equiv \frac{y}{\phi(\theta)}$$

Define $f(\bar{y})$ such that:

$$\bar{T}(y) = \bar{T}(\bar{y}\ \phi(\theta)) \equiv \theta f(\bar{y})$$

Note that $\phi(\theta)$, which is a measure of the shock thickness, is some unknown function of the shock strength. Also note, that the new dependent variable is magnified by some function of the shock strength which in this case must be θ itself. With these substitutions equation (28) becomes:

$$(30) \qquad \frac{\theta}{\phi(\theta)} \frac{df}{d\bar{y}} = \theta^2 f - \theta^2 f^2$$

Clearly in order to balance the differential term, both the linear and quadratic terms are required since they are of the same order in the small parameter θ. Also, the shock thickness must be inversely proportional to the shock strength:

$$(31) \qquad \phi = \frac{1}{\theta}$$

Finally equation (30) can be solved for $f(\bar{y})$ to yield:

$$(32) \qquad f(\bar{y}) = \frac{1}{2} + \frac{1}{2} \tanh \frac{\bar{y}}{2}$$

When the original variables are resubstituted the shock structure is found to be:

$$(33) \qquad T(x) = \frac{1}{2}(T_1 + T_0) + \frac{1}{2}(T_1 - T_0) \tanh \frac{2x}{\delta}$$

$$(34) \qquad \delta = \frac{4a_{II}^2 A}{b\theta}$$

The profile of a second sound shock wave given by equation (33) has the same shape as an ordinary pressure shock profile for weak shock waves. Also the form of the shock thickness, δ, is totally analogous to the ordinary weak shock case which has been calculated by Landau[4]. In both cases the shock thickness is inversely proportional to the shock strength--in the second sound shock case this parameter is the temperature jump divided by the temperature of the initial rest state. Also in both cases the shock thickness includes a thermodynamic coefficient whose sign determines whether the shock is a compression or expansion. For ordinary pressure shocks this coefficient is the "fundamental derivative of gas dynamics", $(\partial^2 p/\partial V^2)_s$, (where V is specific volume). For the second sound case this coefficient is the thermodynamic function b(p,T) defined by equation (24).

The analogy is made complete by the constant terms of proportionality which are equal to the absorption of sound per frequency squared. Khalatnikov[5] has shown that the absorption of second sound is given by:

$$(35) \qquad \alpha = \tfrac{1}{2}\omega^2 \frac{1}{\rho a_{II}^3} \left[\frac{\kappa}{C} + \frac{\rho_s}{\rho_n} \left(\frac{4}{3}\eta + \zeta_2 - 2\rho\zeta_1 + \rho^2\zeta_3 \right) \right]$$

thus

$$(36) \qquad A = \frac{2\alpha}{\omega^2}$$

At first thought such a complete analogy between ordinary pressure shock waves and temperature shock waves in a superfluid may seem surprising since the basic equations of motion as well as the thermodynamics of He II

are very different from those of an ordinary fluid. This analogy however is not a coincidence, but is due to the fact that in both cases the steady profile of a shock wave is due to a balance of the nonlinear steepening effects by dissipative mechanisms. Furthermore it can be shown quite generally, that when a steady wave is formed by balancing nonlinear steepening with some dissipative process-whether it be heat conduction, viscosity, or diffusion,--the result will be a shock wave whose thickness is inversely proportional to the shock strength.

As stated previously, there are two basic types of second sound shock waves--temperature raising and temperature lowering--whose occurrence depends on the sign of $b(p,T)$. As saturated vapor pressure and for a temperature above $1.88^{o}K$ $b(p,T)$ is negative (see figure 1); in this region temperature lowering shocks occur. Below $1.88^{o}K$ to about $0.9^{o}K$, $b(p,T)$ is positive, which requires that second sound shock waves be temperature raising in nature.

A curious phenomenon happens where $b(p,T)$ passes thru zero. Here the shock thickness diverges as a simple pole because $b(p,T)$ resides in the denominator of δ (see Eq. 34). A plot of the shock thickness, normalized by w, is included as figure 2. It should be remarked that near the infinity in shock thickness the analysis is strictly valid only for infinitisimal shock strengths, that is for $\theta \to 0$. This is because the first order correction to the wave velocity, $\frac{1}{2}b(p,T)\theta$, becomes zero at this point making higher order terms important. However the existence of the infinity will not disappear, but only be shifted in temperature by a higher order analysis. The reason this must happen is directly

related to the fact that the shock velocity must equal the characteristic velocities, both in front and back of the shock, at some temperature and amplitude, θ. When this happens there is no energy feeding the shock front, which dictates that a steady profile can only be maintained if the wave is dissipationless. This can only occur if the gradients vanish; that is, the shock thickness must become infinite.

Near temperatures where $b(p,T) = 0$ the shock thickness will become relatively large which will aid experimental investigations of the shock structure. However, to get a larger shock thickness requires a longer time for the shock to steepen into a steady state. With this constraint in mind, the shock thickness could be adequately measured and hence compared with the theoretical value.

REFERENCES

1. Landau, L. and Lifshitz, E. Fluid Mechanics, 1959, Chapter 16.

2. Khalatnikov, I. Introduction to the Theory of Superfluidity, 1965, Chapter 9.

3. Khalatnikov, I. Ibid., Chapter 13.

4. Landau, L. and Lifshitz, E. Fluid Mechanics, 1959, p. 87.

5. Khalatnikov, I. Introduction to the Theory of Superfluidity, 1965, Chapter 12.

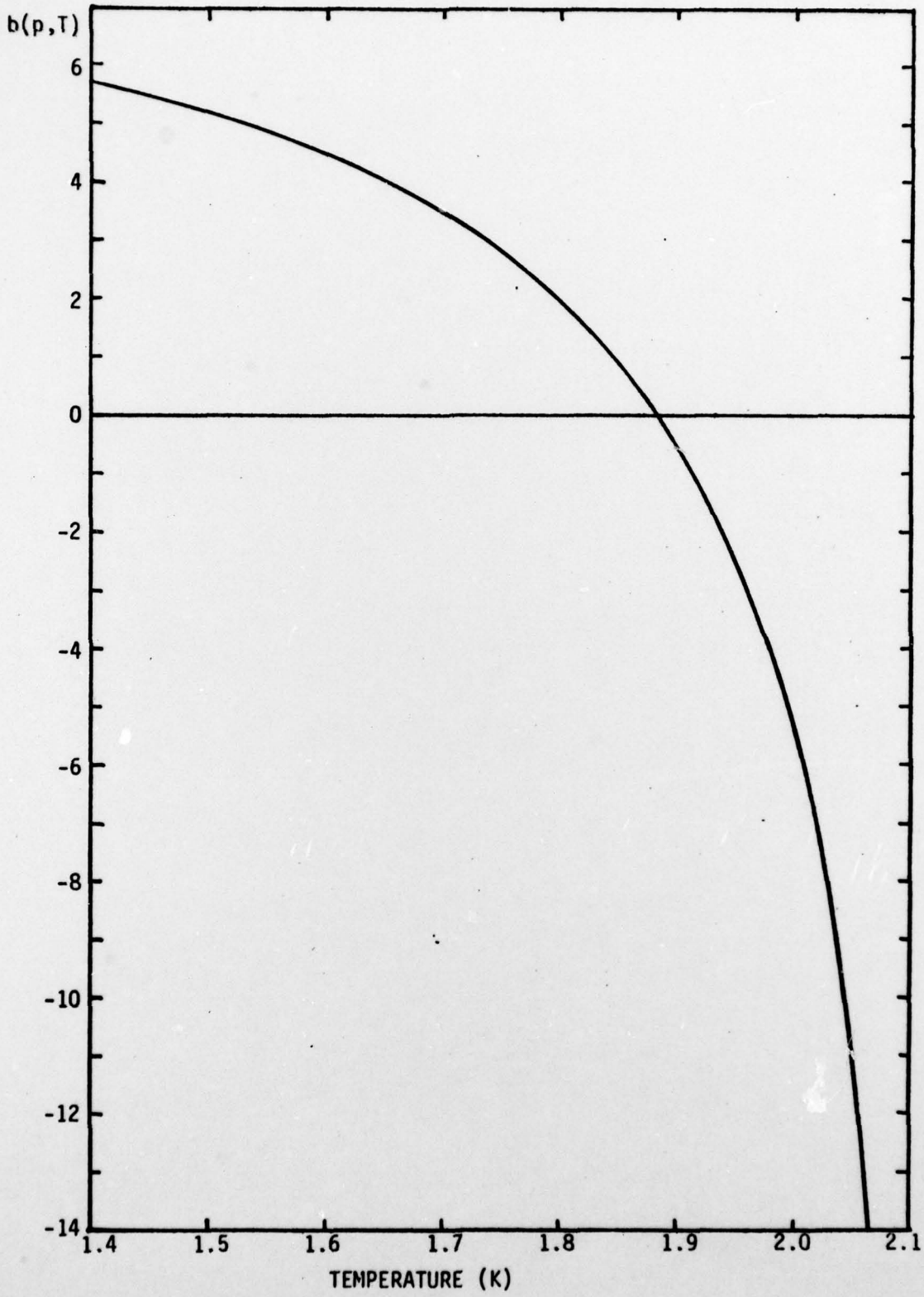

Figure 1. The thermodynamic function b(p,T) at SVP.

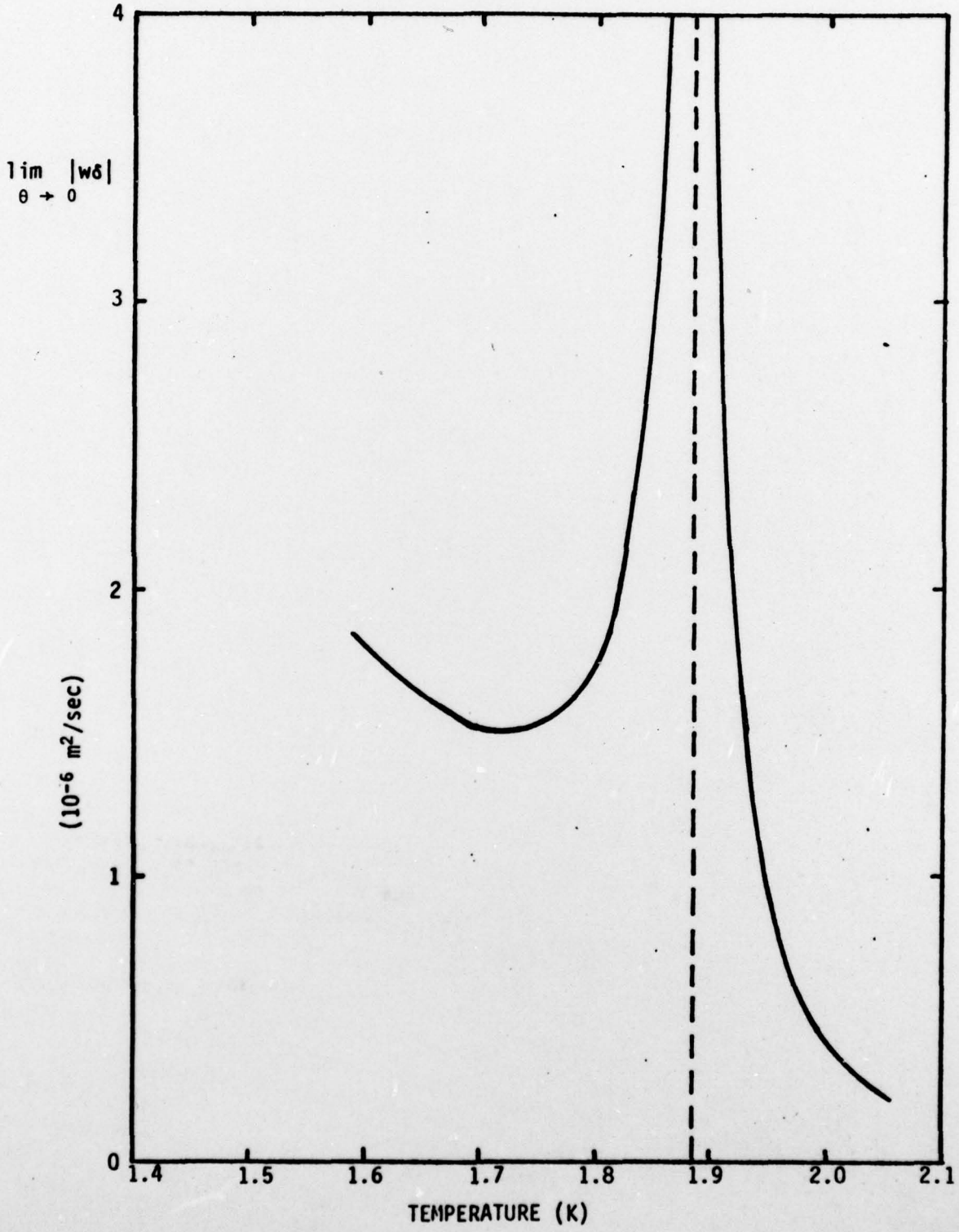

Figure 2. Shock thickness in the limit of vanishing amplitude.

UNCLASSIFIED

SECURITY CLASSIFICATION OF THIS PAGE *(When Data Entered)*

REPORT DOCUMENTATION PAGE	READ INSTRUCTIONS BEFORE COMPLETING FORM
1. REPORT NUMBER **AFOSR-TR- 79-0130** 2. GOVT ACCESSION NO.	3. RECIPIENT'S CATALOG NUMBER
4. TITLE *(and Subtitle)* NONLINEAR INTERACTIONS IN SUPERFLUID DYNAMICS: SUPERCRITICAL COUNTERFLOW AND SHOCKWAVES	5. TYPE OF REPORT & PERIOD COVERED Final
	6. PERFORMING ORG. REPORT NUMBER
7. AUTHOR(s) H W Liepmann, Jack L Wise, Philip L Rogers, Timonthy N Turner	8. CONTRACT OR GRANT NUMBER(s) F44620-75-C-0038
9. PERFORMING ORGANIZATION NAME AND ADDRESS Graduate Aeronautical Laboratories, California Institute of Technology, Pasadena, CA 91109	10. PROGRAM ELEMENT, PROJECT, TASK AREA & WORK UNIT NUMBERS 61102F 2301/A5
11. CONTROLLING OFFICE NAME AND ADDRESS AFOSR/NP, Bolling AFB, Bldg. #410, Washington, DC 20332	12. REPORT DATE Nov 1978
	13. NUMBER OF PAGES 109
14. MONITORING AGENCY NAME & ADDRESS *(if different from Controlling Office)*	15. SECURITY CLASS. *(of this report)* unclassified
	15a. DECLASSIFICATION/DOWNGRADING SCHEDULE

16. DISTRIBUTION STATEMENT *(of this Report)*

Approved for public release; distribution unlimited.

DISTRIBUTION STATEMENT A
Approved for public release; Distribution Unlimited

17. DISTRIBUTION STATEMENT *(of the abstract entered in Block 20, if different from Report)*

18. SUPPLEMENTARY NOTES

19. KEY WORDS *(Continue on reverse side if necessary and identify by block number)*

20. ABSTRACT *(Continue on reverse side if necessary and identify by block number)*

It was the purpose of the program to investigate some aspects of the fluid mechanics of LHeII, in particular nonlinear phenomena such as turbulence and shock waves and their effect on the critical conditions in HeII. The major accomplishments which resulted from the GALCIT research program are: ~~(1)~~ The development of the first cryogenic shock tube for the production of strong shock waves. In this small (1 inch diameter) tube, shock Mach numbers of M = 42 in Helium gas have been reached; ~~(2)~~ The extension of the cryogenic tube techniques to work with liquid Helium II led to the first careful

DD FORM 1 JAN 73 1473 EDITION OF 1 NOV 65 IS OBSOLETE

UNCLASSIFIED

mapping of the nonlinear wave diagrams in He II, involving both first sound and second sound shock waves; (3) Ultra-second sound waves with frequencies up to 1 MHz have been used as a velocimeter for He II counterflow; (4) A similarity rule was developed on the two-fluid equation with the additional Gorter-Mellink terms. This rule permits the reduction of all known critical heat flow experiments in capillaries and tubes to a single number reminiscent of a critical Reynolds number for laminar-turbulent transition in classical fluid mechanics.